Supporting information for "Solubility of organic salts in solvent-antisolvent mixtures: A combined experimental and molecular dynamics simulations approach"

Zoran Bjelobrk,[†] Ashwin Kumar Rajagopalan,[‡] Dan Mendels,[¶] Tarak Karmakar,[§]
Michele Parrinello,[*,‖] and Marco Mazzotti[*,†]

†*Institute of Energy and Process Engineering, ETH Zürich, CH-8092, Switzerland*

‡*Department of Chemical Engineering, University of Manchester, Manchester, M13 9PL, United Kingdom*

¶*Pritzker School of Molecular Engineering, University of Chicago, Chicago, Illinois 60637, United States*

§*Department of Chemistry, Indian Institute of Technology, Delhi, Hauz Khas, New Delhi 110016, India*

‖*Istituto Italiano di Tecnologia (IIT), Via Morego, 30, 16163 Genova GE, Italy*

E-mail: michele.parrinello@iit.it; marco.mazzotti@ipe.mavt.ethz.ch

Contents

S1 Force fields

In this work we have used the general AMBER force fields (GAFF)[1,2] for all our solvent and antisolvent molecules. The force fields have full atomistic description and the bonds involving hydrogens were fixed at their equilibrium value. Force field parameters for MeOH and MeCN were taken from van der Spoel *et al.*[3] and the NaOAc force fields were taken from Kashefolgheta *et al.*[4] The propan-1-ol and sodium acetate force fields are discussed in the following two Sections S1.1 and S1.2.

S1.1 Propan-1-ol force field

The electrostatic potential of propan-1-ol was calculated with Gaussian 09[5] at the B3LYP/6-31G(d,p) level and the partial charges were fitted to the restrained electrostatic potential charges.[6,7] The obtained GAFF parameters of propan-1-ol are listed in Table S1 and the corresponding structural formula with the atom names used in Table S1 is shown in Figure S1e.

To roughly estimate the force field's ability to reproduce reality, we compare the density of a simulated propan-1-ol liquid with the experimental density of $\rho^{\text{exp}}_{\text{PrOH}} = 799.5$ kg/m^3 at ambient conditions.[8] We have therefore performed a simulation run of a box containing 350 liquefied propan-1-ol molecules using Gromacs 2016.5. The simulation was performed at NPT conditions with the Parrinello-Rahman barostat[9] using isotropic pressure coupling and the velocity rescale thermostat[10] at $p = 1$ bar and $T = 298.15$ K. The simulation was run with periodic boundary conditions. The simulated liquid has an average density of $\rho^{\text{sim}}_{\text{PrOH}} = 789.2$ kg/m^3, which was averaged over 25 ns, and is in reasonable accordance with experiment (-1.29 % difference).

Table S1: GAFF parameters for propan-1-ol.

atom name	GAFF atom type	RESP charge [e]	mass [g/mol]	x [nm]	y [nm]	z [nm]
CP1	c3	-0.265718	12.010	-0.178	0.037	0.121
HP1	hc	0.054899	1.008	-0.214	-0.062	0.148
HP2	hc	0.054899	1.008	-0.263	0.096	0.086
HP3	hc	0.054899	1.008	-0.137	0.084	0.210
CP2	c3	0.164627	12.010	-0.070	0.026	0.011
HP4	hc	-0.003642	1.008	-0.113	-0.024	-0.076
HP5	hc	-0.003642	1.008	0.012	-0.035	0.047
CP3	c3	0.361627	12.010	-0.018	0.165	-0.029
HP6	h1	-0.048986	1.008	-0.100	0.226	-0.067
HP7	h1	-0.048986	1.008	0.026	0.215	0.058
OP1	oh	-0.750180	16.000	0.081	0.151	-0.131
HP8	ho	0.430202	1.008	0.113	0.239	-0.155

S1.2 Sodium acetate force fields

For the NaOAc ion pair, force fields reported by Kashefolgheta *et al.*[4] were used, which are comprised of GAFF compatible parameters. The force field of AcO$^-$ is optimized with

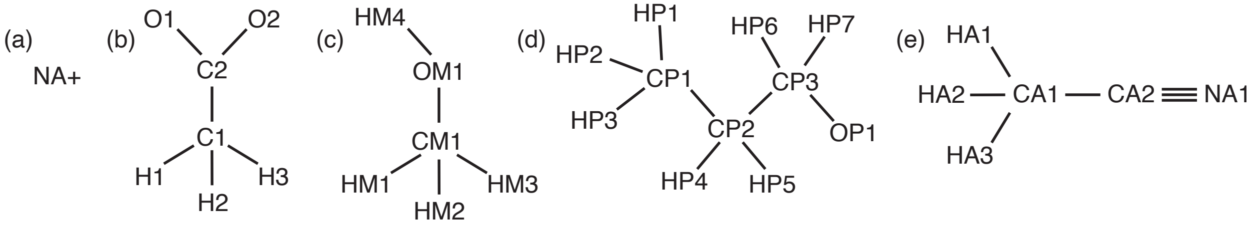

Figure S1: Structural formulas with the used atom names for: a) sodium ion, b) acetate ion, c) methanol, d) propan-1-ol, and e) acetonitrile.

the TIP3P water model[11] and Na^+ model of Joung *et al.*[12] to reproduce experimental hydration- and solvation free energies at low solute concentrations (0.5 M). Unoptimized GAFF parameters for NaOAc would overestimate the ion-ion and ion-solvent interactions. The interested reader is referred to Reference 4 for further details.

As we are dealing here with the crystalline NaOAc phase as well, we require a force field which is capable of reproducing the experimental melting temperature of NaOAc, and not primarily solvation free energies in water. Since the reported NaOAc force fields overestimate the experimental melting temperature, $T_{\mathrm{m}}^{\mathrm{exp}}$, considerably by over 300 K, we need to perform a further fix-up of the force fields for our purposes of obtaining reliable solubility estimates for NaOAc. Without scaling, the solubility predictions will provide results at least an order of magnitude smaller than experiments (see also Section S7). We therefore linearly scale the partial charges of the NaOAc atoms by a scaling factor, $0 < q < 1$, to reduce the simulated NaOAc melting temperature, $T_{\mathrm{m}}^{\mathrm{sim}}$, to meet the experimental one, $T_{\mathrm{m}}^{\mathrm{exp}} = 597$ K.[13] Charge scaling is commonly used to improve the performance of coulombic interactions of non-polarizable force fields in condensed matter simulations and to make them more realistic.[14,15]

To obtain the melting temperature of the NaOAc force fields for a given q we use crystal-melt coexistence MD simulations.[16] Figure S2a shows a representative visualization of the simulation box at the beginning of the simulation, where a crystal of the anhydrous sodium acetate polymorph I is exposed to a sodium acetate melt using periodic boundary conditions.

The initial crystal has roughly the dimensions of 3 × 2.5 × 3 nm^3 and occupies a third of the simulation box volume, while the other two thirds are occupied by the melt. The crystal face {200} was exposed to the melt since it is a fast growing face which allows us to observe growth or dissolution of the crystal within simulation times of 50 ns. Figures S2b and S2c show visualizations of the final configuration of the fully grown and fully dissolved crystalline phase respectively. The simulations were performed under NPT conditions with the velocity rescale thermostat[10] and the Parrinello-Rahman barostat[9] at $p = 1$ bar using semi-isotropic pressure coupling. Only the box length L_z perpendicular to the crystal surface was allowed to change, while box lengths L_x and L_y parallel to the crystal surface were fixed at equilibrium distances.

For each q, sets of individual simulations at different T were performed and the results are listed in Table S2: the value $q = 0.807$ was identified to produce a force fields melting point of $T_\mathrm{m}^\mathrm{sim} = 596$ K, which is in good agreement with its experimental counterpart. The scaled charges of the NaOAc force fields[4] are listed in Table S3 and the corresponding structural formulas with the atom names are shown in Figures S1a and S1b.

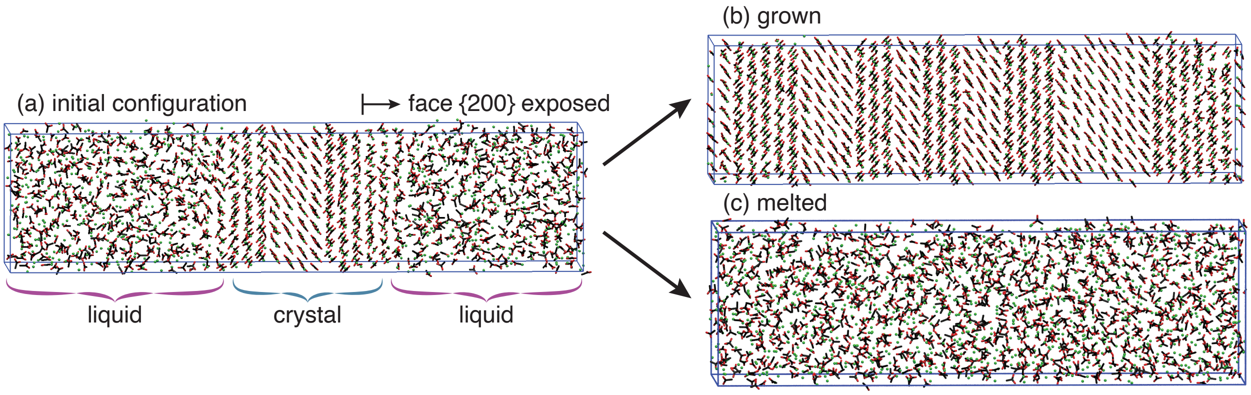

Figure S2: Visualizations of NaOAc crystal-melt coexistence simulations. a) Initial configuration with a crystalline phase (in the center of the box) submerged in the melted phase. b) Fully grown crystalline phase. c) Fully dissolved crystalline phase.

The NaOAc force fields scaled with $q = 0.807$ were tested to see whether they can reproduce the experimental crystal structure. A simulation of the NaOAc polymorph I was

Table S2: Individual coexistence NaOAc crystal-melt simulation outcomes for different charge scaling factors q and simulation temperatures T. d indicates full dissolution of the crystalline phase and g indicates full growth of the crystalline phase. Out of the tested values, $q = 0.807$ provides the best agreement with the experimental melting point of $T_{\mathrm{m}}^{\mathrm{exp}} = 597$ K.[13]

q	595 K	596 K	597 K	598 K	599 K	600 K	605 K	630 K	635 K	640 K
0.805	d					d				
0.806	d									
0.807	g	d	d			d				
0.808	g		g	g	d	d	d			
0.809	g	g	g			g	d			
0.810	g					g	d			
0.840						g		g	g	d

Table S3: Scaled charges used for the NaOAc force fields.[4]

atom name	AMBER atom type	scaled charge [e]
C1	CT	-0.171567
H1	HC	0.002887
H2	HC	0.002887
H3	HC	0.002887
C2	C	0.712154
O1	OACE	-0.678124
O2	OACE	-0.678124
NA+	NA+	0.807000

therefore performed and compared to the experimental crystallographic data.[17] Anhydrous NaOAc polymorph I is orthorhombic and belongs to the *Pcca* space group.

A crystal of roughly the dimensions 3.5 × 3.0 × 2.5 nm^3 containing 288 NaOAc ion pairs was prepared using the experimental atom positions obtained from XRD measurement[17] as initial condition. Figure S3a shows the initial condition (experimental positions of NaOAcs) of the crystal. The simulation was then performed for 50 ns with periodic boundary conditions at $p = 1$ bar and $T = 298$ K using the anisotropic Parrinello-Rahman barostat[9] and the velocity rescale thermostat.[10]

The resulting averaged unit cell lengths, a_{u}, b_{u}, and c_{u} and unit cell volume V_{u} of the simulation are listed and compared to experiments in Table S4. Only the last 25 ns were used for the averaging. The corresponding visualization of time averaged NaOAcs positions within the crystal are shown in Figure S3b. From Table S4 and Figure S3 we can conclude that the NaOAc force fields can reasonably well reproduce the experimental polymorph values.

Table S4: Simulated vs. experimental[17] unit cell lengths, a_u, b_u, and c_u, and unit cell volumes, V_u, of sodium acetate polymorph I (orthorhombic, *Pcca* space group).

	experiment	simulation	difference
a_u	1.7850 nm	1.8136 nm	1.60 %
b_u	0.9982 nm	0.9657 nm	-3.26 %
c_u	0.6068 nm	0.6219 nm	2.49 %
V_u	1.0812 nm^3	1.0892 nm^3	0.74 %

However, the length b_u, which is along the C2-NA+ axis, is slightly underestimated in the simulations while lengths a_u and c_u are slightly overestimated. To understand this discrepancy between simulations and experiments we further computed the energy minimized structures for an ion pair and an ion pair dimer with the NaOAc force fields and compared them to DFT calculations. The results are visualized in Figure S4. The energy minimization of the NaOAc force fields was performed with Gromacs 2016.5[18] with the conjugate gradient algorithm with a tolerance of the maximum force of 0.001 kJ mol^{-1} nm^{-1}. DFT calculations were performed with Gaussian structural optimization routine at the B3LYP/6-31G(d,p) level.[5] The AcO$^-$-Na$^+$ interaction is underestimated in the force fields as the distances between the AcO$^-$ oxygens and Na$^+$ are shorter in the DFT calculations (2.18 Å) compared to the force fields (2.30 Å, see Figure S4a). For the ion pair dimer (see Figure S4b), the distances between AcO$^-$ oxygens and Na$^+$ are as well shorter in the DFT calculations (2.14, 2.38, and 2.23 Å) when compared to the force fields (2.30, 2.47, and 2.29 Å). This coincides with observation, that the unit cell lengths a_u and c_u are longer in simulations compared to the experiments. Contrariwise, the AcO$^-$-AcO$^-$ distance is longer in the DFT calculation (3.29 Å for the nearest oxygens) than it is for the force fields' calculation (3.12 Å), which coincides with the observation of a slightly shorter unit cell length b_textu in simulations compared to experiments.

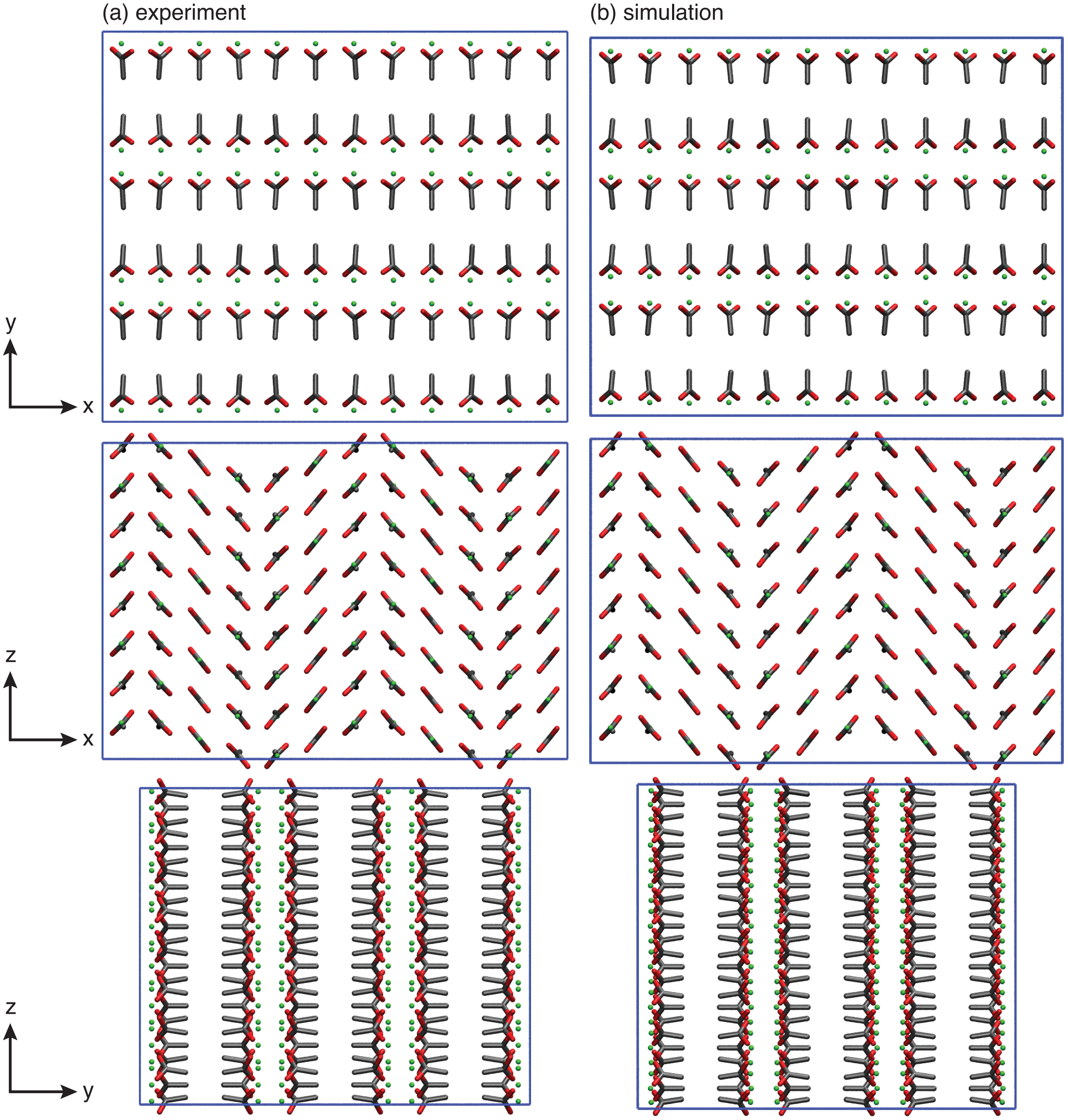

Figure S3: NaOAc crystal visualizations projected along z, y, and x directions. The green spheres denote Na^+ and AcO^-'s oxygens and carbons are colored in red and black respectively. Hydrogens are omitted for clarity. The blue lines denote the simulation box edges. a) Atom positions from the experimental XRD data. b) Averaged atom positions of the NPT simulation.

Overall, the scaled NaOAc force fields reproduce reasonably well the crystallographic data.

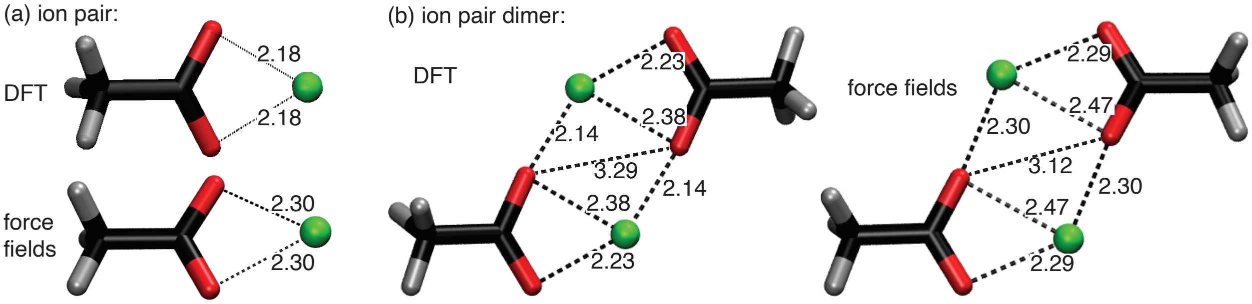

Figure S4: Visualization of the energy minimized structures for a) NaOAc ion pair and b) NaOAc ion pair dimers in vacuum calculated with DFT (top) and the scaled NaOAc force fields (bottom). The same color scheme of the atoms as in Figure S3 is used, where hydrogen molecules are colored in grey. Atom distances between the atoms, indicated with dashed lines, are given in Å.

S2 Simulation setup and equilibration

In this work, we performed kink growth and dissolution sampling of Na^+ and AcO^- at the NaOAc crystal kink site in solvent/antisolvent mixtures in accordance with the reported experiments. Namely in pure MeOH, 80-20% MeOH-PrOH, 60-40% MeOH-PrOH, 40-60% MeOH-PrOH, 75-25% MeOH-MeCN, and 50-50% MeOH-MeCN. The simulation box specifications for the six systems are listed in Table S5. At high antisolvent concentrations, i.e. 40-60% MeOH-PrOH and 50-50% MeOH-MeCN, larger simulation boxes were used in order to be able to reach with the CμMD algorithm sufficiently low concentrations of NaOAc in solution. Each simulation box is comprised of a NaOAc polymorph I[17] crystal slab exposing face {200} to the solution, whereas the top surface is comprised of an unfinished surface layer containing an unfinished row with kink sites. Figure S5 shows visualizations of the simulation boxes of all six studied systems. The corresponding unfinished surface layers are shown in Figure S6. The unfinished surface layer was cut along the [010] direction. Along this edge of the particular face {200}, Na^+ and AcO^- are linearly arranged as dimers, which allows us to focus on the minimum of two types of growth and dissolution processes. Namely one for each of the two ions, in order to extract the solute concentration dependent energy difference between grown and dissolved ion at the corresponding kink site, $\Delta F_{\mathrm{Na+}}$ and $\Delta F_{\mathrm{AcO-}}$. With their sum, $\Delta F = \Delta F_{\mathrm{Na+}} + \Delta F_{\mathrm{AcO-}}$, which corresponds to the energy difference for the dimeric unit, we can consequently identify the solubility as the mole fraction, χ, where $\Delta F = 0$, as discussed in the main text.

Table S5: Simulation box specifications of the studied systems.

	pure MeOH	MeOH-PrOH			MeOH-MeCN	
	100%	80-20%	60-40%	40-60%	75-25%	50-50%
N_{AcONa} [-]	139	131	129	228	129	228
N_{MeOH} [-]	580	495	363	488	446	646
N_{MeCN} [-]	0	0	0	0	116	504
N_{PrOH} [-]	0	66	129	390	0	0
L_x [nm]	2.48781	2.48781	2.48781	3.73161	2.48781	3.73161
L_y [nm]	2.89733	2.89733	2.89733	3.86232	2.89733	3.86232
L_z [nm]	7.12771	7.42265	7.28108	7.14148	7.32957	7.80798
T [K]	300	300	300	300	300	300
p [bar]	1	1	1	1	1	1

We shall now explain how the reported simulation configurations were generated. Each equilibration simulation reported in this work was performed with Gromacs 2016.5.[18] All simulations were run with full atomistic description, periodic boundary conditions, particle mesh Ewald approach[19,20] for the calculation of electrostatic interactions, where the non-bonded cutoff was set to 1 nm. The covalent bonds involving hydrogens were constrained at their equilibrium distances using the LINCS algorithm.[21,22] To equilibrate the simulation boxes to the desired temperature and pressure, the velocity rescaling thermostat[10] and Parrinello-Rahman barostat[9] were used respectively.

In a first step, the seed crystal of the NaOAc polymorph I was generated from XRD data[17] with face {200} perpendicular to the z axis. The crystal system energy was then minimized with the conjugate gradient algorithm with a maximum force tolerance of 50 kJ mol^{-1} nm^{-1}. The energy minimized crystal structure was then thermally equilibrated for 1 ns

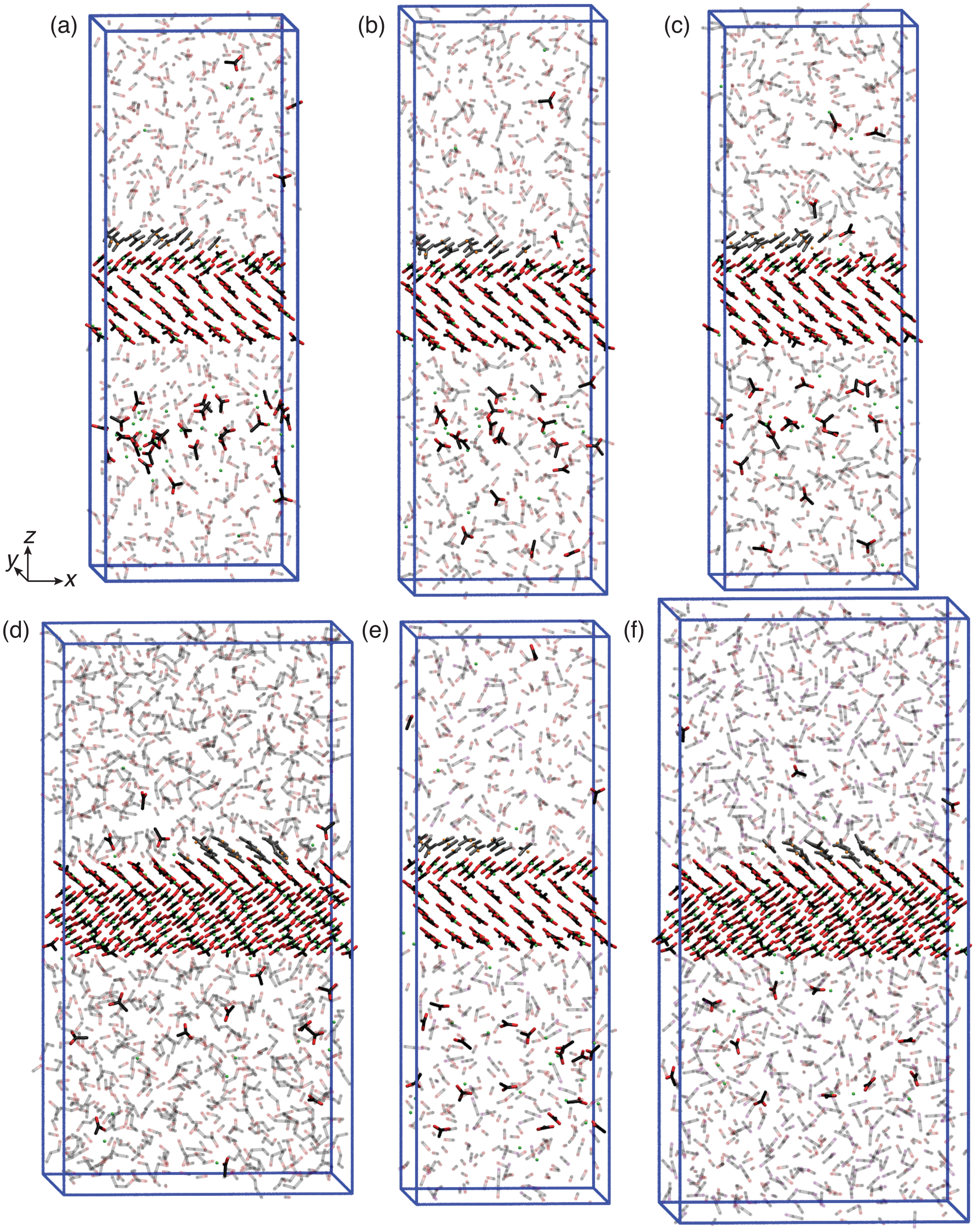

Figure S5: Visualizations of simulation boxes used for Na^+ growth and dissolution simulations in each of the investigated solvent/antisolvent mixtures. The biased kink site can be found in the middle of each upper crystal surface. a) shows the case for a pure MeOH, b) 80-20% MeOH-PrOH, c) 60-40% MeOH-PrOH, d) 40-60% MeOH-PrOH, e) 75-25% MeOH-MeCN, and f) the 50-50% MeOH-MeCN solution. The Na^+ and AcO^- in the unfinished surface layer are colored in grey, while all other Na^+ ions are colored in green. Carbons are colored in black, oxygens in red, and nitrogens in purple. The solvent and antisolvent molecules are shown in faded colors. Hydrogens are omitted for clarity.

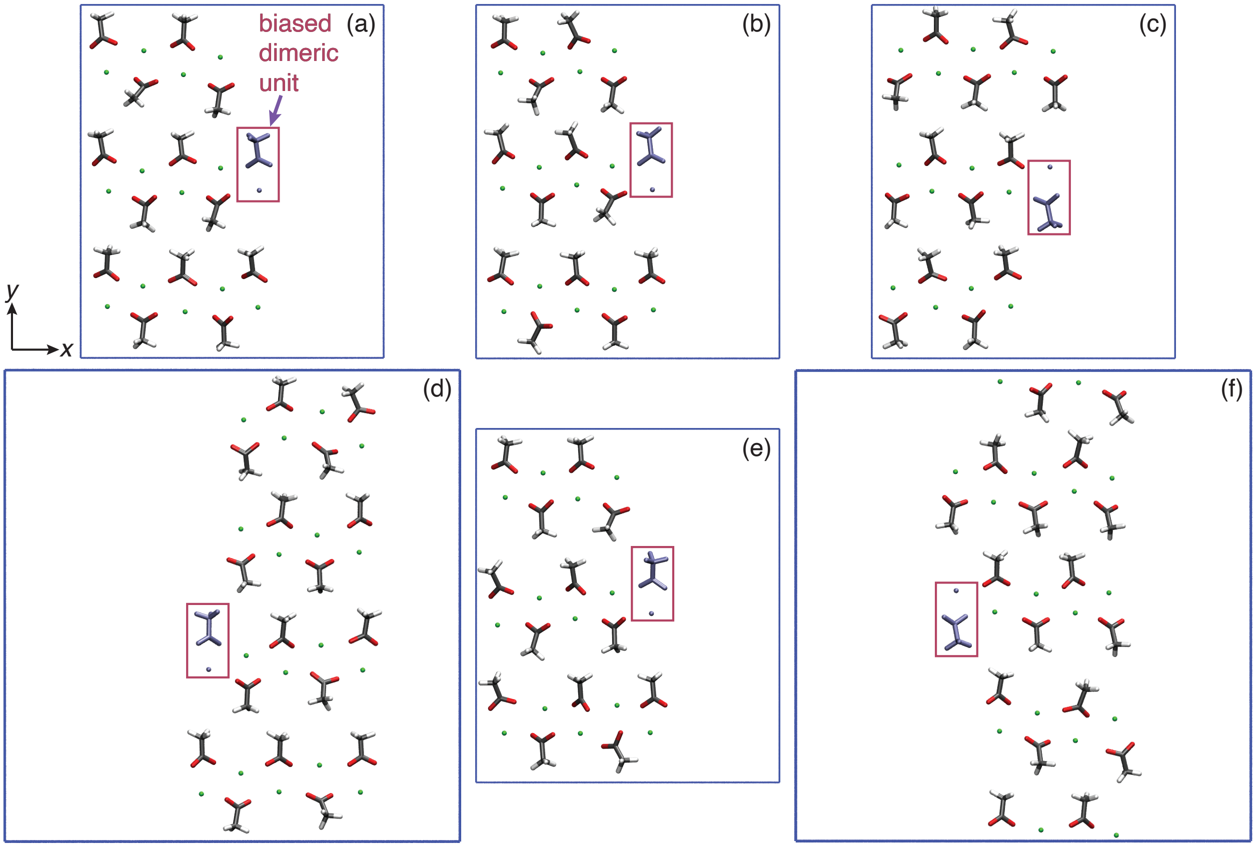

Figure S6: Visualizations of the unfinished surface layers, seen along the z axis perpendicular to the crystal surface, for a) 100% MeOH, b) 80-20% MeOH-PrOH, c) 60-40% MeOH-PrOH, d) 40-60% MeOH-PrOH, e) 75-25% MeOH-MeCN, and f) 50-50% MeOH-MeCN. Na^+ are colored in green, carbons in black, oxygens in red and hydrogens in light grey. The NaOAc dimeric unit, comprising the biased kink sites of Na^+ and AcO^-, is colored in blue and framed in red.

at NVT conditions with a time integration step of 0.5 fs to reach the target temperature of $T = 300$ K. The crystal system pressure was then equilibrated to the targeted 1 bar at NPT conditions with the anisotropic Parrinello-Rahman barostat using a time integration step of 0.5 fs. After the pressure equilibration of 5 ns, the simulation was continued for further 20 ns to sample the average box lengths L_x and L_y and to identify the simulation frame closest to these average lengths, which was used as seed crystal in the following step.

The seed crystal with the averaged L_x and L_y box lengths was submerged in the particular NaOAc, solvent, and antisolvent solution using the Gromacs genbox utility.[22] We expose only face $\{200\}$ to the solution. Face $\{200\}$ is perpendicular to the z axis of the simulation box. The simulation box energy minimization and temperature equilibration were performed in the same fashion as for the crystal system. The pressure equilibration was performed for 5 ns at NPT conditions using the semi-isotropic Parrinello-Rahman barostat, where we allowed the box to change in size along the z axis while keeping the already averaged L_x and L_y box lengths constant. The simulation was continued for another 20 ns, from which the average box length L_z was sampled. The simulation frame closest to L_z was used as initial condition for the final preparation step.

In the final step we have used the CμMD algorithm[23] to generate the desired concentration profiles in the bulk liquid. Further details on the CμMD algorithm are discussed in the following Section S3. During the solution concentration equilibration, a potential was introduced through adsorption site CVs (discussed in Section S4.1) which pushed all Na^+ and AcO^- ions, which do not belong to the unfinished surface layer, away from the crystal surface. The unfinished surface layer ions were prevented from dissolving by the use of harmonic potentials introduced through surface structure CVs, which are discussed in Section S4.2. The center of mass of the two most inner layers was fixed with a harmonic potential to prevent the drift of the crystal. This drift would be undesirable for our setup. Simulation times of 50 ns ensure well equilibrated solute concentration profiles.

S3 Constant chemical potential method

To keep the chemical potential of NaOAc constant in the vicinity of the crystal surface comprising the kink site, the CμMD algorithm[23] is introduced.

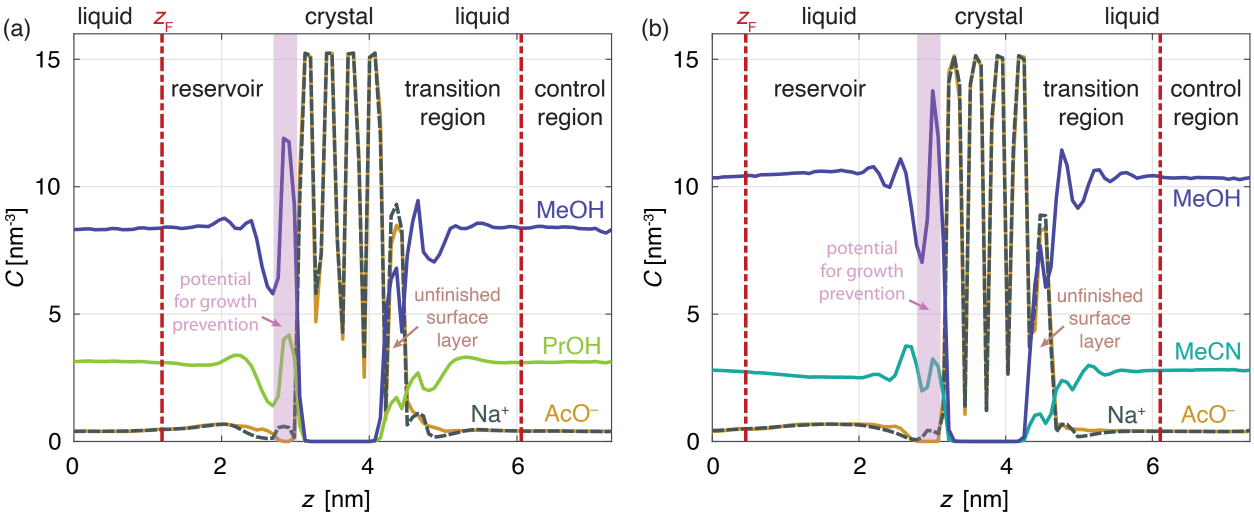

Figure S7: Concentration profiles of each species, given in number of ions or molecules per nm^{-3}, along the z axis for two representative simulation runs. a) NaOAc in 60-40% MeOH-PrOH with an AcO$^-$ control region target concentration $C_0 = 0.4$ nm^{-3}. b) NaOAc in 75-25% MeOH-MeCN with an AcO$^-$ control region target concentration $C_0 = 0.5$ nm^{-3}. The blue lines correspond to the MeOH, green lines to PrOH, turquoise lines to MeCN, brown lines to AcO$^-$ and dashed grey lines to Na$^+$ concentration profiles. The boundaries between the different liquid compartments, i.e. transition region, control region, and reservoir, are marked with red vertical dashed lines, whereas the position of the external force field is marked by z_{F}. The crystal with 4 fully grown layers (4 Na$^+$ and AcO$^-$ density peaks) is positioned in the center. The unfinished surface layer is shown on the right side of the crystal with an AcO$^-$ peak of maximum concentration $C = 8$ nm^{-3}. The action region of the potential, which prevents the opposite crystal surface from growing, is shaded in light purple. The concentration profiles were averaged over 1.2 μs of simulations.

We shall briefly discuss the function of the CμMD algorithm. As shown in Figure S7, the liquid phase of the system is segmented into 3 different parts along the z axis perpendicular to the crystal surface: the transition region, control region and reservoir. The transition region starts at the crystal-liquid interface and finishes where the concentration gradient of the solute becomes zero. The transition region is followed by the control region in which the CμMD algorithm tracks the concentration of solute molecules, $C_{\mathrm{CR}}(t)$, at each time instant t.

If $C_{\mathrm{CR}}(t)$ is below the target concentration, C_0, an external force, F_i^{μ}, acts at the interface between the control region and reservoir at position z_{F}. F_i^{μ} is defined as follows

$$F_i^{\mu} = k^{\mu}(C_{\mathrm{CR}}(t) - C_0)G_{\omega}(z_i, z_{\mathrm{F}}). \tag{S1}$$

$G_{\omega}(z_i, z_{\mathrm{F}})$ is a bell shaped function

$$G_{\omega}(z_i, z_{\mathrm{F}}) = \frac{1}{4\omega}\left[1 + \cosh\left(\frac{z_i - z_{\mathrm{F}}}{\omega}\right)\right]^{-1}. \tag{S2}$$

ω defines the height and width of the bell curve. F_i^{μ} will accelerate solute molecules from the reservoir towards the control region, if C_{CR} is smaller than C_0. If C_{CR} is larger than C_0, F_i^{μ} will accelerate the solute molecules out of the control region towards the reservoir. This ensures a constant solute concentration in the control region and allows us to run growth and dissolution simulations at constant chemical potential.

To prevent the growth of the crystal surface on the opposite site of the one containing the kink site, a harmonic potential is introduced (see Figure S7). The potential acts through adsorption site CVs, which are discussed in Section S4.1, and prevents ions dissolved in the reservoir from adsorbing at the surface. At the same time, the surface layer is prevented from dissolving by the use of another harmonic potential and surface structure CVs, which are discussed in Section S4.2. The crystal morphology is not affected by these potentials.

The CμMD algorithm was initially developed for a binary non-ionic molecular system and later extended to a three component aqueous rock salt solution.[24] In this work however we apply the algorithm to a quaternary liquid system involving two ions, a solvent and an antisolvent. Despite this more complicated liquid phase, the CμMD algorithm is able to keep the chemical potential constant as shown in Figures S7a and S7b showing the time averaged subspecies concentration profiles for the cases 60-40% MeOH-PrOH and 75-25% MeOH-MeCN respectively. Even if the ions are mostly dissociated in the solution, we track and accelerate only the AcO$^-$ with the CμMD algorithm, since the Na$^+$ are following the diffusion movement of AcO^- due to the coulombic attraction of the ions. In both Figures S7a and S7b the concentration curves of AcO^- and Na^+ overlap. The targeted concentration profiles in the control region are met for both the NaOAc concentration, as well as for the desired solvent-antisolvent concentration ratio with excellent accuracy. The CμMD parameters used for each simulation setup are reported in Table S6.

Table S6: Values of the CμMD parameters. Length parameters are given in fractional coordinates.

	pure MeOH	MeOH-PrOH			MeOH-MeCN	
	100%	80-20%	60-40%	40-60%	75-25%	50-50%
ω/L_z [-]	0.02	0.02	0.02	0.02	0.02	0.02
z_{TR}/L_z [-]	0.20	0.24	0.24	0.24	0.20	0.20
z_{CR}/L_z [-]	0.30	0.33	0.33	0.31	0.30	0.33
z_{F}/L_z [-]	0.52	0.59	0.59	0.57	0.52	0.55
$\Delta z/L_z$ [-]	1/120	1/120	1/120	1/120	1/120	1/120

S4 Collective variables (CVs)

S4.1 Adsorption site CVs

In the biased simulation runs we aim to sample many growth and dissolution events of the biased kink site to obtain the needed convergence accuracy. As discussed in Section S5, the time to acquire enough growth and dissolution events is in the order of 1.5 μs for the studied NaOAc systems. Although the growth of NaOAc at kinks and edges of the unfinished surface layer is slow in unbiased simulations, in a time span of 1.5 μs this process is highly likely to occur. And this growth at other adsorption sites around the biased kink site can disrupt and slow down the sampling performance of the biased simulation.

To prevent the growth of NaOAc at other sites apart from the biased kink site, we introduce harmonic potential walls through adsorption site CVs. We use two types of adsorption site CVs, namely spherical ones for single adsorption sites such as kinks and prismatic ones for edges. The spherical adsorption site CVs are defined with logistic step functions for a particular adsorption site a and ion type as follows:

$$s_{a,\mathrm{ion}} = \sum_i \left(1 - \frac{1}{1 + \exp(-\sigma_a(|\mathbf{r}_i - \mathbf{r}_a| - d_a))} \right), \tag{S3}$$

where σ_a and d_a define the steepness of the step and radius of the adsorption site respectively, $\mathbf{r}_i$ is the position of ion i, and $\mathbf{r}_a$ corresponds to the position of adsorption site a.

The edge adsorption site CVs are also comprised of logistic switching functions and have following functional form for a particular ion type

$$\begin{aligned} s_{\varsigma,\mathrm{ion}} = \sum_i \Bigg[& \frac{1}{1 + \exp(-\sigma_\varsigma(x_i - x_\mathrm{l}))} \left(1 - \frac{1}{1 + \exp(-\sigma_\varsigma(x_i - x_\mathrm{u}))} \right) \\ & \cdot \frac{1}{1 + \exp(-\sigma_\varsigma(z_i - z_\mathrm{l}))} \left(1 - \frac{1}{1 + \exp(-\sigma_\varsigma(z_i - z_\mathrm{u}))} \right) \Bigg]. \end{aligned} \tag{S4}$$

σ_ς dictates the steepness of the step functions. x_i and z_i are the positions of ion i along the x and z axis. x_l and x_u, as well as z_l and z_u are intervals which confine the adsorption site CV's region of action along the x and z axis.

Harmonic wall potentials are introduced through the spherical adsorption site CVs

$$V_{a,\mathrm{ion}} = \begin{cases} 0, & \text{if } s_a < s_{a,0}, \\ k_a(s_a - s_{a,0})^2, & \text{else,} \end{cases} \tag{S5}$$

and edge adsorption site CVs:

$$V_{\varsigma,\mathrm{ion}} = \begin{cases} 0, & \text{if } s_\varsigma < s_{\varsigma,0}, \\ k_\varsigma(s_\varsigma - s_{\varsigma,0})^2, & \text{else,} \end{cases} \tag{S6}$$

where k_a and k_ς are the force constants and $s_{a,0}$ and $s_{\varsigma,0}$ are the threshold values of the adsorption site CVs beyond which the bias potentials start to act.

The adsorption site CV parameters used for each simulation setup are listed in Table S7 for the Na^+ ions and Table S8 for the AcO^- ions. Spherical adsorption sites are enumerated from $a = 1$ to 4. The center of mass of the oxygen atoms O1 and O2 are defined as the AcO^- ion positions. The adsorption site CVs with the reported parameters are positioned along all edges and kinks except for the biased kink site. These configurations of potentials allow us to keep the biased kink site environment intact for the time span necessary to obtain converged free energy profiles. The force constants of the potentials are set as mild as possible in order not to disturb ions from diffusing through these sites. Figure S8 shows the contour lines of the adsorption site CVs, $s_{1,\mathrm{Na+}}$, $s_{2,\mathrm{Na+}}$, $s_{3,\mathrm{Na+}}$, $s_{4,\mathrm{Na+}}$ $s_{\varsigma,\mathrm{Na+}}$, $s_{1,\mathrm{AcO-}}$, $s_{2,\mathrm{AcO-}}$, $s_{3,\mathrm{AcO-}}$, $s_{4,\mathrm{AcO-}}$, and $s_{\varsigma,\mathrm{AcO-}}$, used for the pure MeOH solution simulation setup.

S4.2 Surface structure CVs

During the NaOAc kink growth and dissolution simulations, it is likely that ions of crystal layers, which are exposed to solution, dissolve and alter the environment of the biased kink site. That would disrupt the sampling of the growth and dissolution events at the particular kink site.

To prevent such undesired dissolution of ions that belong to crystal layers at the crystal-solution interface, harmonic potential walls are introduced for each of these layers, l, and for each ion type through surface structure CVs, $s_{\mathrm{st},l,\mathrm{ion}}$. $s_{\mathrm{st},l,\mathrm{ion}}$ is defined as a logistic function

$$s_{\mathrm{st},l,\mathrm{ion}} = \frac{1}{1+\exp\left(-\sigma_{\mathrm{st}}(\tilde{s}_{\mathrm{st}} - \tilde{s}_{\mathrm{st},0})\right)}, \tag{S7}$$

where $\tilde{s}_{\mathrm{st},0}$ denotes the step position and σ_{st} the steepness of following function

$$\tilde{s}_{\mathrm{st,ion}} = \sum_i \left(\sum_k \left[\cos^{\eta_x}\left(\frac{\nu_x \pi}{L_x}(x_i - \bar{x}_k)\right) \cos^{\eta_y}\left(\frac{\nu_y \pi}{L_y}(y_i - \bar{y}_k)\right) \right] \exp\left\{ -\frac{(z_i - \bar{z}_k)^2}{2\sigma_z^2} \right\} \right). \tag{S8}$$

Along the xy plane we introduce sinusoidal functions which capture the lattice positions of

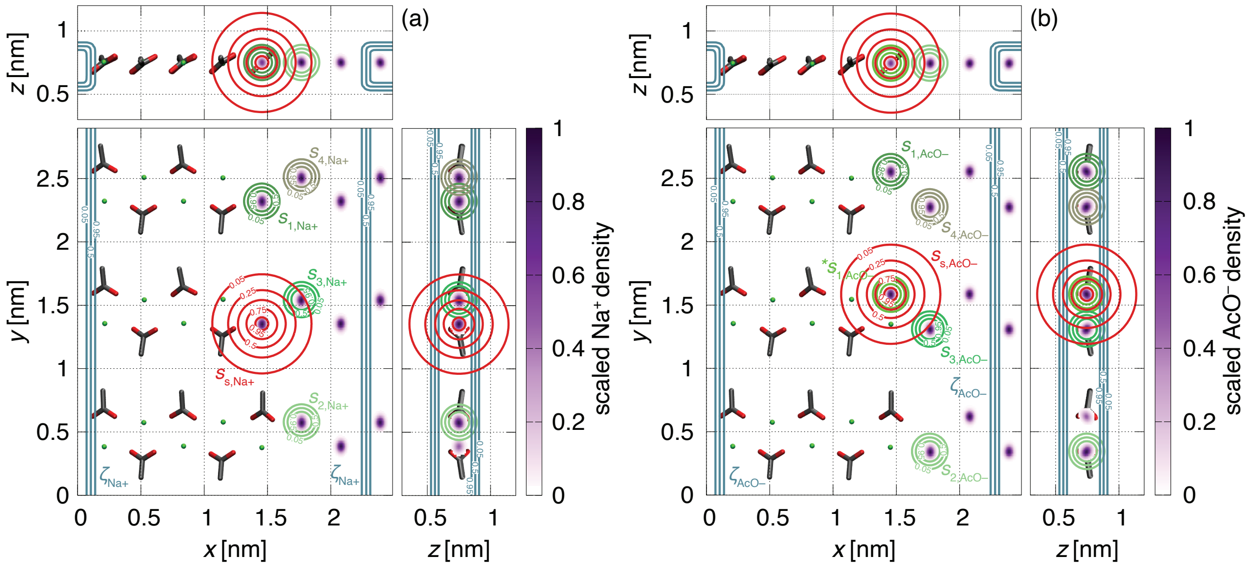

Figure S8: Contour lines of the adsorption site CVs (green lines) shown for a) adsorption sites of Na^+ and b) adsorption sites of AcO^- on the crystal surface comprising the biased kink site. The adsorption site CVs are the ones used for the pure MeOH solution simulation setup and their contour lines are shown at values of 0.01, 0.5, and 0.99. Contour lines of the Gaussian like functions, $s_{\mathrm{s,Na+}}$ in a) and $s_{\mathrm{s,s,AcO\text{-}}}$ in b), which are the kink site ion density terms in the biased CVs $s_{\mathrm{b,Na+}}$ and $s_{\mathrm{b,AcO\text{-}}}$ respectively, are colored in red. The contours are shown as projections along all three coordinates. The unfinished surface layer ions are presented with structural formulas using the same color code as in Figure S5 (hydrogens are omitted for clarity). The histograms belong to the scaled crystalline ion densities, a) Na^+ and b) AcO^-, of the surface layer which are not part of the unfinished surface layer and are sampled from 50 ns of unbiased simulations. These NaOAc crystalline positions overlap with the adsorption sites. The AcO^- ion positions are defined as the center of mass of their two oxygens. The histograms were scaled by their maximum density values.

Table S7: Values of adsorption site CVs for Na^+. The coordinate origin of the z axis is set to the box center.

		pure MeOH	MeOH-PrOH			MeOH-MeCN	
		100%	80-20%	60-40%	40-60%	75-25%	50-50%
s_{1,Na^+}	$r_a^{(x)}$ [nm]	1.4584	1.4576	1.4567	1.6569	1.4587	1.3433
	$r_a^{(y)}$ [nm]	2.3234	2.3232	0.5792	2.3287	2.3242	1.0640
	$r_a^{(z)}$ [nm]	0.7506	0.6860	0.7562	0.7514	0.8713	0.7505
	σ_a [-]	100	100	100	100	100	100
	d_a [nm]	0.11	0.11	0.11	0.11	0.11	0.11
	k_a [kJ/mol]	40	40	40	40	40	40
	$s_{a,0}$ [-]	0.1	0.1	0.1	0.1	0.1	0.1
s_{2,Na^+}	$r_a^{(x)}$ [nm]	1.7687	1.7702	1.7676	1.6569	1.7690	1.3433
	$r_a^{(y)}$ [nm]	0.5786	0.5792	0.3908	3.2839	0.5785	0.0915
	$r_a^{(z)}$ [nm]	0.7506	0.6860	0.7562	0.7514	0.8713	0.7505
	σ_a [-]	100	100	100	100	100	100
	d_a [nm]	0.11	0.11	0.11	0.11	0.11	0.11
	k_a [kJ/mol]	20	20	20	20	20	20
	$s_{a,0}$ [-]	0.1	0.1	0.1	0.1	0.1	0.1
s_{3,Na^+}	$r_a^{(x)}$ [nm]	1.7687	1.7702	1.7676	1.3455	1.7690	1.0329
	$r_a^{(y)}$ [nm]	1.5442	1.5439	1.3590	0.5666	1.5430	2.8151
	$r_a^{(z)}$ [nm]	0.7506	0.6860	0.7562	0.7514	0.8713	0.7505
	σ_a [-]	100	100	100	100	100	100
	d_a [nm]	0.11	0.11	0.11	0.11	0.11	0.11
	k_a [kJ/mol]	20	20	20	20	20	20
	$s_{a,0}$ [-]	0.1	0.1	0.1	0.1	0.1	0.1
s_{4,Na^+}	$r_a^{(x)}$ [nm]	1.7687	1.7702	1.7676	1.3455	1.7690	-
	$r_a^{(y)}$ [nm]	2.5123	2.5090	2.3227	3.4620	2.5098	-
	$r_a^{(z)}$ [nm]	0.7506	0.6860	0.7562	0.7514	0.8713	-
	σ_a [-]	100	100	100	100	100	-
	d_a [nm]	0.11	0.11	0.11	0.11	0.11	-
	k_a [kJ/mol]	20	20	20	20	20	-
	$s_{a,0}$ [-]	0.1	0.1	0.1	0.1	0.1	-
$\varsigma_{\mathrm{Na}^+}$	σ_ς [-]	100	100	100	100	100	100
	x_l [nm]	1.0371	1.0361	1.0365	1.1753	1.0369	0.8539
	x_u [nm]	1.3471	1.3461	1.3465	1.5053	1.3469	1.1739
	z_l [nm]	0.5600	0.4960	0.5662	0.5584	0.6813	0.5606
	z_u [nm]	0.8800	0.8060	0.8762	0.8884	0.9913	0.8906
	k_ς [kJ/mol]	25	25	25	25	25	25
	ς_0 [nm]	0.5	0.5	0.5	0.5	0.5	0.5

Table S8: Values of adsorption site CVs for AcO$^-$. The coordinate origin of the z axis is set to the box center.

		pure MeOH	MeOH-PrOH			MeOH-MeCN	
		100%	80-20%	60-40%	40-60%	75-25%	50-50%
s_{0,AcO^-}	$r_a^{(x)}$ [nm]	1.4571	1.4576	1.4559	1.6577	1.4583	1.3449
	$r_a^{(y)}$ [nm]	1.5908	1.5911	1.3103	1.5981	1.5916	1.7992
	$r_a^{(z)}$ [nm]	0.7442	0.6794	0.7496	0.7484	0.8639	0.7476
	σ_a [-]	100	100	100	100	100	100
	d_a [nm]	0.11	0.11	0.11	0.11	0.11	0.11
	k_a [kJ/mol]	40	40	40	40	40	40
	$s_{a,0}$ [-]	0.1	0.1	0.1	0.1	0.1	0.1
s_{1,AcO^-}	$r_a^{(x)}$ [nm]	1.4571	1.4576	1.4559	1.6577	1.4583	1.3449
	$r_a^{(y)}$ [nm]	2.5567	2.5567	0.3459	2.5621	2.5573	3.7210
	$r_a^{(z)}$ [nm]	0.7442	0.6794	0.7496	0.7484	0.8639	0.7476
	σ_a [-]	100	100	100	100	100	100
	d_a [nm]	0.11	0.11	0.11	0.11	0.11	0.11
	k_a [kJ/mol]	40	40	40	40	40	40
	$s_{a,0}$ [-]	0.1	0.1	0.1	0.1	0.1	0.1
s_{2,AcO^-}	$r_a^{(x)}$ [nm]	1.7674	1.7683	1.7682	1.6577	1.7687	1.3449
	$r_a^{(y)}$ [nm]	0.3452	0.3459	0.6245	3.5243	0.3452	0.8306
	$r_a^{(z)}$ [nm]	0.7442	0.6794	0.7496	0.7484	0.8639	0.7476
	σ_a [-]	100	100	100	100	100	100
	d_a [nm]	0.11	0.11	0.11	0.11	0.11	0.11
	k_a [kJ/mol]	20	20	20	20	20	20
	$s_{a,0}$ [-]	0.1	0.1	0.1	0.1	0.1	0.1
s_{3,AcO^-}	$r_a^{(x)}$ [nm]	1.7674	1.7683	1.7682	1.3462	1.7687	1.0343
	$r_a^{(y)}$ [nm]	1.3125	1.3095	1.5934	1.3102	1.3097	2.0772
	$r_a^{(z)}$ [nm]	0.7442	0.6794	0.7496	0.7484	0.8639	0.7476
	σ_a [-]	100	100	100	100	100	100
	d_a [nm]	0.11	0.11	0.11	0.11	0.11	0.11
	k_a [kJ/mol]	20	20	20	20	20	20
	$s_{a,0}$ [-]	0.1	0.1	0.1	0.1	0.1	0.1
s_{4,AcO^-}	$r_a^{(x)}$ [nm]	1.7674	1.7683	1.7682	1.3462	1.7687	-
	$r_a^{(y)}$ [nm]	2.2782	2.2764	2.5563	0.3431	2.2767	-
	$r_a^{(z)}$ [nm]	0.7442	0.6794	0.7496	0.7484	0.8639	-
	σ_a [-]	100	100	100	100	100	-
	d_a [nm]	0.11	0.11	0.11	0.11	0.11	-
	k_a [kJ/mol]	20	20	20	20	20	-
	$s_{a,0}$ [-]	0.1	0.1	0.1	0.1	0.1	-
$\varsigma_{\mathrm{AcO}^-}$	σ_ς [-]	100	100	100	100	100	100
	x_l [nm]	1.0357	1.0359	1.0361	1.1753	1.0362	0.8339
	x_u [nm]	1.3457	1.3459	1.3461	1.5053	1.3462	1.1540
	z_l [nm]	0.5542	0.4894	0.5596	0.5584	0.6739	0.5542
	z_u [nm]	0.8642	0.7994	0.8696	0.8884	0.9839	0.8642
	k_ς [kJ/mol]	25	25	25	25	25	25
	ς_0 [nm]	0.5	0.5	0.5	0.5	0.5	0.5

the ions. η_x and η_y define the widths of the peaks and need to be even positive integers. ν_x and ν_y correspond to the number of unit cells along the x and y axis. L_x and L_y are the simulation box lengths in the x and y dimensions. $\bar{x}_k$ and $\bar{y}_k$ is the k-th ion position in the xy unit cell plane. Along the z axis of the simulation box, where we have no continuous crystal periodicity, we introduce Gaussian functions. $\bar{z}_k$ defines the average position of ion k in z direction of the simulation box and σ_z defines the width of the Gaussian functions. The terms are summed over each ion i that belongs to the corresponding layer l.

Harmonic wall potentials are introduced for each $s_{\mathrm{st},l,\mathrm{ion}}$ in the following form

$$V_{\mathrm{st},l,\mathrm{ion}} = \begin{cases} k_{\mathrm{st}}(s_{\mathrm{st}} - s_{\mathrm{st},0})^2, & \text{if } s_{\mathrm{st}} < s_{\mathrm{st},0}, \\ 0, & \text{else.} \end{cases} \tag{S9}$$

k_{st} is the force constant and $s_{\mathrm{st},0}$ denotes the threshold value below which the harmonic potential starts to act.

The shape of $s_{\mathrm{st},l,\mathrm{ion}}$ is chosen such that ions in the given crystalline layer are not affected by the harmonic potential as long as the ions are within their crystal lattice position. This is the case where $s_{\mathrm{st},l,\mathrm{ion}} = 1$ for the given ion i. $s_{\mathrm{st},l,\mathrm{ion}}$ should have values below 1 only when the ion i is outside its lattice position. It is important that $V_{\mathrm{st},l,\mathrm{ion}}$ does not interfere with the natural lattice vibrations of the crystal. This is achieved by setting the parameters of $s_{\mathrm{st},l,\mathrm{ion}}$ such that for each ion i at its vibration amplitude position $s_{\mathrm{st},l,\mathrm{ion}}$ still has a value of 1. If the vibrations are hindered, the simulations give distorted growth and dissolution processes. The vibration amplitudes can be obtained from unbiased simulations of the crystal exposed to solution. Figures S9a and S9b show the contour lines of $s_{\mathrm{st},l,\mathrm{ion}}$ together with the histograms of the ion positions of the unfinished surface layer for Na^+ and AcO^-. For AcO^-, the oxygen positions are considered. The contour lines show that $s_{\mathrm{st},l,\mathrm{ion}}$ only has values below 1 at a distance where the ion density approaches values of zero.

In the biased simulations we applied potential walls to the unfinished surface layer, $s_{\mathrm{st},5,\mathrm{ion}}$, the layer adjacent to the unfinished surface layer, $s_{\text{st},4,\text{ion}}$, and the layer on the opposite crystal surface, $s_{\text{st},1,\text{ion}}$. The appropriate parameter values are listed in Tables S9, S10, S11, S12, S13, and S14.

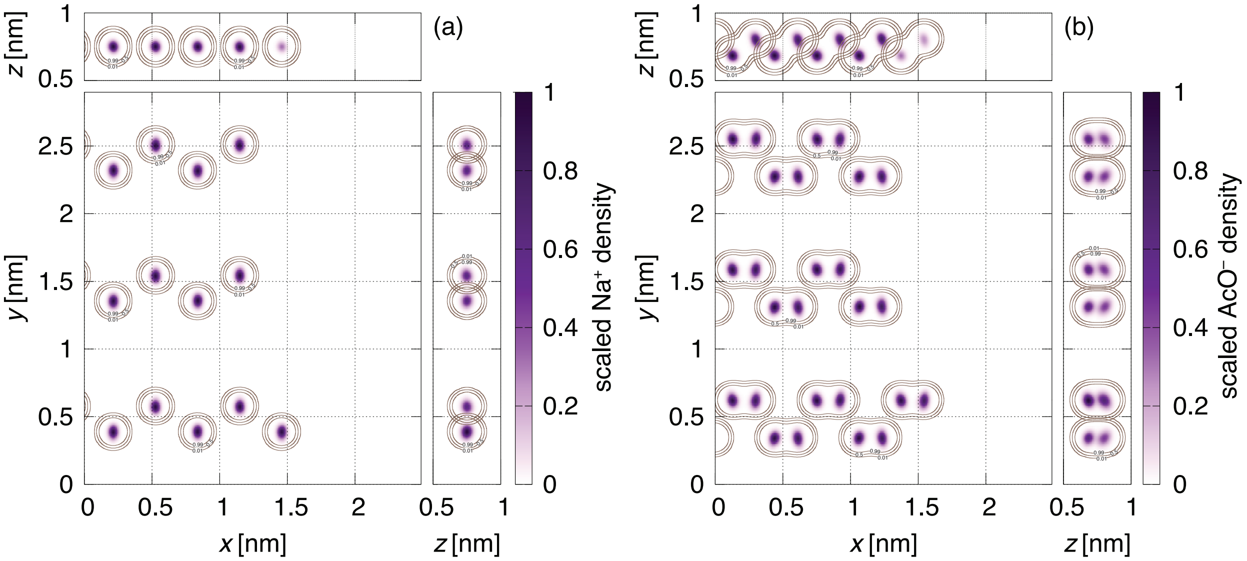

Figure S9: Contour lines of the surface structure CVs (brown lines) for a) Na^+ and b) AcO^- used in the pure MeOH simulation setups. The contour lines are shown at values of 0.01 (most outer rings), 0.5, and 0.99 (most inner rings). The histograms correspond to the scaled densities of a) Na^+ ions and b) AcO^- oxygens which belong to the unfinished surface layer. The histograms were sampled from 50 ns of unbiased simulation and scaled by their maximum density values.

S4.3 Biased CVs

Since the growth and dissolution of Na^+ as well as AcO^- are rare events, we need to enhance the process by applying WTMetaD to overcome the timescale limitations and obtain sufficient growth and dissolution events. Only with sufficient sampling can we reliably compute the energy difference between grown and dissolved dimeric unit states. The slow degrees of freedom for the ions of organic salts are the same ones as for organic molecules, which we have investigated in our previous work.[25] These are the diffusion of the solute to the kink site, the desorption of the solvent from the particular site, and the partial desolvation and

Table S9: Values of the surface structure CV parameters for Na^+ of the unfinished surface layer. $^{*)}$In the Na^+ kink growth simulations, a $s_{\mathrm{st},0}$ value of 13 or 17 was used. For kink growth simulations of AcO^-, the Na^+ of the biased dimeric unit was kept in its crystalline position with the surface structure CV using a $s_{\mathrm{st},0}$ value of 14 or 18.

	pure MeOH	MeOH-PrOH			MeOH-MeCN	
	100%	80-20%	60-40%	40-60%	75-25%	50-50%
ν_x [-]	4	4	4	6	4	6
L_x [nm]	2.48781	2.48781	2.48781	3.73161	2.48781	3.73161
η_x [-]	10	10	10	10	10	10
$\bar{x}_1$ [nm]	-0.7199	-0.7184	-0.7184	-0.2089	-0.7188	2.2765
$\bar{x}_2$ [nm]	-0.4080	-0.4080	-0.4080	0.1017	-0.4069	2.5884
ν_y [-]	3	3	3	4	3	4
L_y [nm]	2.89733	2.89733	2.89733	3.86232	2.89733	3.86232
η_y [-]	26	26	26	26	26	26
$\bar{y}_1$ [nm]	-1.0579	-0.8695	-0.8695	-3.4640	-0.8699	-2.9848
$\bar{y}_2$ [nm]	-0.8694	-1.0572	-1.0572	-3.2855	-1.0580	-2.7983
$\bar{z}_1$ [nm]	0.7562	0.6860	0.6860	0.7514	0.8713	0.7506
$\bar{z}_2$ [nm]	0.7562	0.6860	0.6860	0.7514	0.8713	0.7506
σ_z [nm]	0.06	0.06	0.06	0.06	0.06	0.06
σ_{st} [-]	150	150	150	150	150	150
$\tilde{s}_{\mathrm{st},0}$ [-]	0.10	0.10	0.10	0.10	0.10	0.10
k_{st} [kJ/mol]	25	25	25	25	25	25
$s_{\mathrm{st},0}$ [-]	13/14*	13/14*	13/14*	17/18*	13/14*	17/18*

Table S10: Values of the surface structure CV parameters for AcO$^-$ of the unfinished surface layer.

	pure MeOH	MeOH-PrOH			MeOH-MeCN	
	100%	80-20%	60-40%	40-60%	75-25%	50-50%
ν_x [-]	4	4	4	6	4	6
L_x [nm]	2.48781	2.48781	2.48781	3.73161	2.48781	3.73161
η_x [-]	12	12	12	12	12	12
$\bar{x}_1$ [nm]	-0.9452	-0.9439	-0.9439	-0.2943	-0.9446	-1.5411
$\bar{x}_2$ [nm]	-0.8049	-0.8037	-0.8037	-0.1228	-0.8018	-1.3676
$\bar{x}_3$ [nm]	-0.6332	-0.6339	-0.6339	0.0161	-0.6323	-1.2288
$\bar{x}_4$ [nm]	-0.4927	-0.4926	-0.4926	0.1887	-0.4931	-1.0572
ν_y [-]	3	3	3	4	3	4
L_y [nm]	2.89733	2.89733	2.89733	3.86232	2.89733	3.86232
η_y [-]	30	30	30	30	30	30
$\bar{y}_1$ [nm]	-0.8256	-0.8244	-0.8244	-0.3335	-0.8244	0.1454
$\bar{y}_2$ [nm]	-0.1365	-1.1030	-1.1030	-0.3335	-1.1039	0.1454
$\bar{y}_3$ [nm]	-0.1365	-1.1030	-1.1030	-0.6212	-1.1039	-0.1288
$\bar{y}_4$ [nm]	-0.8256	-0.8244	-0.8244	-0.6212	-0.8244	-0.1288
$\bar{z}_1$ [nm]	0.8109	0.7409	0.7409	0.8090	0.9290	0.8092
$\bar{z}_2$ [nm]	0.6929	0.6238	0.6238	0.6960	0.8122	0.6915
$\bar{z}_3$ [nm]	0.8109	0.7409	0.7409	0.8090	0.9290	0.8092
$\bar{z}_4$ [nm]	0.6929	0.6238	0.6238	0.6960	0.8122	0.6915
σ_z [nm]	0.06	0.06	0.06	0.06	0.06	0.06
σ_{st} [-]	0.10	0.10	0.10	0.10	0.10	0.10
$\tilde{s}_{\mathrm{st},0}$ [-]	150	150	150	150	150	150
k_{st} [kJ/mol]	25	25	25	25	25	25
$s_{\mathrm{st},0}$ [-]	26	26	26	34	26	34

Table S11: Values of the surface structure CV parameters for Na^+ of layer 4.

	pure MeOH	MeOH-PrOH			MeOH-MeCN	
	100%	80-20%	60-40%	40-60%	75-25%	50-50%
ν_x [-]	4	4	4	6	4	6
L_x [nm]	2.48781	2.48781	2.48781	3.73161	2.48781	3.73161
η_x [-]	10	10	10	10	10	10
$\bar{x}_1$ [nm]	-0.8335	-0.8341	-0.8341	-1.6510	-0.8328	-1.6517
$\bar{x}_2$ [nm]	-0.5232	-0.5225	-0.5225	-1.3424	-0.5219	-1.3398
ν_y [-]	3	3	3	4	3	4
L_y [nm]	2.89733	2.89733	2.89733	3.86232	2.89733	3.86232
η_y [-]	26	26	26	26	26	26
$\bar{y}_1$ [nm]	-0.1002	-1.0664	-1.0664	-1.5462	-1.0657	-1.0651
$\bar{y}_2$ [nm]	-0.8620	-0.8629	-0.8629	-1.3423	-0.8618	-0.8624
$\bar{z}_1$ [nm]	0.4477	0.3830	0.7830	0.4462	0.5680	0.4467
$\bar{z}_2$ [nm]	0.4477	0.3830	0.3830	0.4462	0.5680	0.4467
σ_z [nm]	0.06	0.06	0.06	0.06	0.06	0.06
σ_{st} [-]	150	150	150	150	150	150
$\tilde{s}_{\mathrm{st},0}$ [-]	0.10	0.10	0.10	0.10	0.10	0.10
k_{st} [kJ/mol]	15	15	15	15	15	15
$s_{\mathrm{st},0}$ [-]	24	24	24	48	24	48

adsorption of the solute at the kink site. We therefore use CVs with the same functional form as the ones reported in Reference 25.

The WTMetaD bias potential is introduced for each ion through the particular biased CV, $s_{\mathrm{b,ion}}$. Each $s_{\mathrm{b,ion}}$ is a set of functions, which are linear combinations of the local density of the particular ion and the local density of solvent and antisolvent molecules at the corresponding kink site of the ion.[25] The densities are defined as sums of Gaussian like bell curve terms; for each ion

$$s_{\mathrm{s,ion}} = \sum_i \exp\left(-\frac{|\mathbf{r}_i - \mathbf{r}_{\mathrm{s,ion}}|^2}{2\sigma^2_{\mathrm{s,ion}}}\right), \tag{S10}$$

and for the corresponding solvent and antisolvent

$$s_{\mathrm{l,ion}} = \sum_j \exp\left(-\frac{|\mathbf{r}_j - \mathbf{r}_{\mathrm{l,ion}}|^2}{2\sigma^2_{\mathrm{l,ion}}}\right). \tag{S11}$$

$\mathbf{r}_i$ and $\mathbf{r}_j$ are the positions of the ion i and solvent or antisolvent j. $\mathbf{r}_{\mathrm{s,ion}}$ is the location of

Table S12: Values of the surface structure CV parameters for AcO$^-$ of layer 4.

	pure MeOH	MeOH-PrOH			MeOH-MeCN	
	100%	80-20%	60-40%	40-60%	75-25%	50-50%
ν_x [-]	4	4	4	6	4	6
L_x [nm]	2.48781	2.48781	2.48781	3.73161	2.48781	3.73161
η_x [-]	12	12	12	12	12	12
$\bar{x}_1$ [nm]	-0.9132	-0.9135	-0.9135	-1.5720	-0.9132	-1.5700
$\bar{x}_2$ [nm]	-0.7531	-0.7525	-0.7525	-1.4248	-0.7527	-1.4215
$\bar{x}_3$ [nm]	-0.6031	-0.6029	-0.6029	-1.2609	-0.6018	-1.2589
$\bar{x}_4$ [nm]	-0.4422	-0.4421	-0.4421	-1.1135	-0.4427	-1.1106
ν_y [-]	3	3	3	4	3	4
L_y [nm]	2.89733	2.89733	2.89733	3.86232	2.89733	3.86232
η_y [-]	30	30	30	30	30	30
$\bar{y}_1$ [nm]	-0.8343	-0.8348	-0.8348	-1.3146	-0.8332	-0.8347
$\bar{y}_2$ [nm]	-0.8343	-0.8348	-0.8348	-1.5738	-0.8332	-1.0952
$\bar{y}_3$ [nm]	-0.1281	-1.0946	-1.0946	-1.5738	-1.0934	-1.0952
$\bar{y}_4$ [nm]	-0.1281	-1.0946	-1.0946	-1.3146	-1.0934	-0.8347
$\bar{z}_1$ [nm]	0.3817	0.3167	0.3167	0.3826	0.5020	0.3832
$\bar{z}_2$ [nm]	0.5153	0.4502	0.4502	0.5159	0.6360	0.5154
$\bar{z}_3$ [nm]	0.3817	0.3167	0.3167	0.3826	0.5020	0.3832
$\bar{z}_4$ [nm]	0.5153	0.4502	0.4502	0.5159	0.6360	0.5154
σ_z [nm]	0.06	0.06	0.06	0.06	0.06	0.06
σ_{st} [-]	150	150	150	150	150	150
$\tilde{s}_{\text{st},0}$ [-]	0.10	0.10	0.10	0.10	0.10	0.10
k_{st} [kJ/mol]	15	15	15	15	15	15
$s_{\text{st},0}$ [-]	48	48	48	96	48	96

Table S13: Values of the surface structure CV parameters for Na^{+} of layer 1.

	pure MeOH	MeOH-PrOH			MeOH-MeCN	
	100%	80-20%	60-40%	40-60%	75-25%	50-50%
ν_x [-]	4	4	4	6	4	6
L_x [nm]	2.48781	2.48781	2.48781	3.73161	2.48781	3.73161
η_x [-]	10	10	10	10	10	10
$\bar{x}_1$ [nm]	-0.9195	-0.9193	-0.9193	-1.2510	-0.9180	-1.2546
$\bar{x}_2$ [nm]	-0.6083	-0.6092	-0.6092	-0.9389	-0.6084	-0.9439
ν_y [-]	3	3	3	4	3	4
L_y [nm]	2.89733	2.89733	2.89733	3.86232	2.89733	3.86232
η_y [-]	26	26	26	26	26	26
$\bar{y}_1$ [nm]	-1.0600	-1.0598	-1.0598	-1.3512	-1.0596	-0.8683
$\bar{y}_2$ [nm]	-0.8655	-0.8682	-0.8682	-0.5760	-0.8676	-0.0939
$\bar{z}_1$ [nm]	-0.4536	-0.5187	-0.5187	-0.4531	-0.3329	-0.4538
$\bar{z}_2$ [nm]	-0.4536	-0.5187	-0.5187	-0.4531	-0.3329	-0.4538
σ_z [nm]	0.06	0.06	0.06	0.06	0.06	0.06
σ_{st} [-]	150	150	150	150	150	150
$\tilde{s}_{\mathrm{st},0}$ [-]	0.10	0.10	0.10	0.10	0.10	0.10
k_{st} [kJ/mol]	15	15	15	15	15	15
$s_{\mathrm{st},0}$ [-]	24	24	24	48	24	48

the ion's adsorption site, and identical with its crystal lattice position at the kink site. $\mathbf{r}_{\mathrm{l,ion}}$ is the adsorption site of the solvent or antisolvent at the solvated kink site. $\mathbf{r}_{\mathrm{s,ion}}$ and $\mathbf{r}_{\mathrm{l,ion}}$ are for the investigated NaOAc kink sites not identical positions. $\sigma_{\mathrm{s,ion}}$ and $\sigma_{\mathrm{l,ion}}$ define the width of each Gaussian like bell curve.

$s_{\mathrm{s,ion}}$ captures the slow coordinate of diffusion and adsorption/desorption of the ion. $s_{\mathrm{l,ion}}$ captures the slow coordinate of desolvation/solvation of the kink site. These functions are combined into the biased CV

$$s_{\mathrm{b,ion}} = w_{\mathrm{s,ion}}(s_{\mathrm{s,ion}}^{\chi_{\mathrm{s1,ion}}} + s_{\mathrm{s,ion}}^{\chi_{\mathrm{s2,ion}}}) + w_{\mathrm{l,ion}} s_{\mathrm{l,ion}}^{\chi_{\mathrm{l,ion}}}. \tag{S12}$$

$w_{\mathrm{s,ion}}$ and $w_{\mathrm{l,ion}}$ are linear weights of each local density. $s_{\mathrm{b,ion}}$ has the same functional form as the one reported in our previous work.[25,26] The performance of the WTMetaD sampling is

Table S14: Values of the surface structure CV parameters for AcO^- of layer 1.

	pure MeOH	MeOH-PrOH			MeOH-MeCN	
%	100	80-20	60-40	40-60	75-25	50-50
ν_x [-]	4	4	4	6	4	6
L_x [nm]	2.48781	2.48781	2.48781	3.73161	2.48781	3.73161
η_x [-]	12	12	12	12	12	12
$\bar{x}_1$ [nm]	-1.0043	-1.0050	-1.0050	-1.1659	-1.0024	-1.1651
$\bar{x}_2$ [nm]	-0.8331	-0.8347	-0.8347	-1.0258	-0.8334	-1.0274
$\bar{x}_3$ [nm]	-0.6922	-0.6924	-0.6924	-0.8546	-0.6917	-0.8600
$\bar{x}_4$ [nm]	-0.5235	-0.5235	-0.5235	-0.7137	-0.5224	-0.7181
ν_y [-]	3	3	3	4	3	4
L_y [nm]	2.89733	2.89733	2.89733	3.86232	2.89733	3.86232
η_y [-]	30	30	30	30	30	30
$\bar{y}_1$ [nm]	-0.8266	-0.8249	-0.8249	-0.6206	-0.8264	-0.1365
$\bar{y}_2$ [nm]	-0.8266	-0.8249	-0.8249	-1.3073	-0.8264	-0.8257
$\bar{y}_3$ [nm]	-0.1371	-0.1350	-0.1350	-1.3073	-1.1017	-0.8257
$\bar{y}_4$ [nm]	-0.1371	-0.1350	-0.1350	-0.6206	-1.1017	-0.1365
$\bar{z}_1$ [nm]	-0.3953	-0.4573	-0.4573	-0.3973	-0.2750	-0.3971
$\bar{z}_2$ [nm]	-0.5096	-0.5739	-0.5739	-0.5090	-0.3897	-0.5096
$\bar{z}_3$ [nm]	-0.3953	-0.4573	-0.4573	-0.3973	-0.2750	-0.3971
$\bar{z}_4$ [nm]	-0.5096	-0.5739	-0.5739	-0.5090	-0.3897	-0.5096
σ_z [nm]	0.06	0.06	0.06	0.06	0.06	0.06
σ_{st} [-]	150	150	150	150	150	150
$\tilde{s}_{\text{st},0}$ [-]	0.10	0.10	0.10	0.10	0.10	0.10
k_{st} [kJ/mol]	15	15	15	15	15	15
$s_{\text{st},0}$ [-]	48	48	48	96	48	96

improved significantly by mapping[27,28] the local densities as follows

$$s_{\mathrm{s,ion}} \rightarrow s_{\mathrm{s,ion}}^{\chi_{\mathrm{s1,ion}}} + s_{\mathrm{s,ion}}^{\chi_{\mathrm{s2,ion}}}, \tag{S13}$$

and

$$s_{\mathrm{l,ion}} \rightarrow s_{\mathrm{l,ion}}^{\chi_{\mathrm{l,ion}}}, \tag{S14}$$

with the scalar positive exponents, $\chi_{\mathrm{s1}} < 1$, $\chi_{\mathrm{s2}} > 1$ and $\chi_{\mathrm{l}} < 1$. The mapping of the density functions allows us firstly, to obtain for the FES, $F(s_{\mathrm{b,ion}})$, broad local energy minima basins of equal widths. This enables us to use a larger Gaussian width of the bias potentials, σ_W, in the WTMetaD simulations, which consequently accelerates convergence. Secondly, the mapping allows us to push $s_{\mathrm{s,ion}}$ and $s_{\mathrm{l,ion}}$ considerably away from values of zero, at which the WTMetaD sampling performance can be otherwise disturbed. More details can be found in Reference 27. Without mapping the density functions appropriately, the biased simulations will not converge.

For the organic compounds involved in the biased CVs of Na$^+$, $s_{\mathrm{b,Na+}}$, and AcO$^-$, $s_{\mathrm{b,AcO-}}$, following ion and molecule centers were defined;

- ◇ AcO$^-$: center of mass of oxygen atoms (O1 and O2),
- ◇ MeOH: oxygen atom (OM1),
- ◇ PrOH: oxygen atom (OP1),
- ◇ MeCN: nitrogen atom (NA1).

From unbiased simulations, one can obtain the orientations and positions of the ions as well as solvent and antisolvent molecules at the kink site. The alcohol oxygens and acetonitrile nitrogen share the same adsorption sites. However, the positions of these solvent and antisolvent adsorption sites differ for Na$^+$ and AcO$^-$.

Contour lines of $s_{\mathrm{s,Na+}}$ and $s_{\mathrm{s,AcO\text{-}}}$ are shown in Figures S8a and S8b respectively.

In simulations involving WTMetaD, it is beneficial to introduce lower and upper wall potentials for the biased CVs to improve the sampling performance. We therefore have used following wall potentials for the biased CVs of each ion

$$V_{\mathrm{s,ion}} = \begin{cases} k_{\mathrm{s,l}}((s_{\mathrm{s}}^{\chi_{\mathrm{s1}}} + s_{\mathrm{s}}^{\chi_{\mathrm{s2}}}) - s_{\mathrm{s,l}})^2, & \text{if } (s_{\mathrm{s}}^{\chi_{\mathrm{s1}}} + s_{\mathrm{s}}^{\chi_{\mathrm{s2}}}) < s_{\mathrm{s,l}}, \\ k_{\mathrm{s,u}}((s_{\mathrm{s}}^{\chi_{\mathrm{s1}}} + s_{\mathrm{s}}^{\chi_{\mathrm{s2}}}) - s_{\mathrm{s,u}})^2, & \text{if } (s_{\mathrm{s}}^{\chi_{\mathrm{s1}}} + s_{\mathrm{s}}^{\chi_{\mathrm{s2}}}) > s_{\mathrm{s,u}}, \\ 0, & \text{else,} \end{cases} \tag{S15}$$

and

$$V_{\mathrm{l,ion}} = \begin{cases} k_{\mathrm{l,l}}(s_{\mathrm{l}}^{\chi_{\mathrm{l}}} - s_{\mathrm{l,l}})^2, & \text{if } s_{\mathrm{l}}^{\chi_{\mathrm{l}}} < s_{\mathrm{l,l}}, \\ k_{\mathrm{l,u}}(s_{\mathrm{l}}^{\chi_{\mathrm{l}}} - s_{\mathrm{l,u}})^2, & \text{if } s_{\mathrm{l}}^{\chi_{\mathrm{l}}} > s_{\mathrm{l,u}}, \\ 0, & \text{else.} \end{cases} \tag{S16}$$

$k_{\mathrm{s,l}}$, $k_{\mathrm{s,u}}$, $k_{\mathrm{l,l}}$, and $k_{\mathrm{l,u}}$ are the force constants and $s_{\mathrm{s,l}}$, $s_{\mathrm{s,u}}$, $s_{\mathrm{l,l}}$, and $s_{\mathrm{l,u}}$ are the thresholds below and above which the potentials are active. Lower walls are necessary to prevent the biased simulations from getting stuck at CV values of zero. Higher walls prevent the biased system from visiting non-physical states of excessive agglomeration of ions or solvent and antisolvent molecules at the kink site.

The parameter values used for the biased CVs are presented in Table S15 and the WTMetaD parameters are listed in Table S16.

S4.4 Crystallinity CVs

To compute the energy difference between crystalline and dissolved kink site states, one requires a measure of the crystallinity of the kink site. The biased CVs, which are designed to capture the slow degrees of freedom of the kink growth and dissolution process, do not define the crystallinity of the kink site. We therefore have to define another set of CVs, which do capture the crystallinity. We define a set of logistic functions, which are of same functional form as the spherical adsorption site CVs discussed in Section S4.1, for a particular atom of

Table S15: Values of the biased CVs used for Na^+ and AcO^- kink growth and dissolution sampling.

		pure MeOH	MeOH-PrOH			MeOH-MeCN	
	%	100	80-20	60-40	40-60	75-25	50-50
$s_{\mathrm{s,Na^+}}$	$r_\mathrm{s}^{(x)}$ [nm]	1.4584	1.4576	1.4567	1.6569	1.4587	1.3433
	$r_\mathrm{s}^{(y)}$ [nm]	1.3558	1.3572	1.5447	1.3601	1.3575	2.0351
	$r_\mathrm{s}^{(z)}$ [nm]	0.7506	0.6860	0.7562	0.7514	0.8713	0.7506
	σ_s [-]	0.16	0.16	0.16	0.16	0.16	0.16
	χ_s [-]	0.3	0.3	0.3	0.3	0.3	0.3
	χ_s [-]	3	3	3	3	3	3
	w_s [-]	0.5	0.5	0.5	0.5	0.5	0.5
	$k_\mathrm{s,l}$ [kJ/mol]	25	25	25	25	25	25
	$k_\mathrm{s,u}$ [kJ/mol]	25	25	25	25	25	25
	$s_\mathrm{s,l}$ [-]	0.02	0.02	0.02	0.02	0.02	0.02
	$s_\mathrm{s,u}$ [-]	2.08	2.08	2.08	2.08	2.08	2.08
$s_{\mathrm{l,Na^+}}$	$r_\mathrm{l}^{(x)}$ [nm]	1.3886	1.3845	1.3845	1.7300	1.3880	1.4240
	$r_\mathrm{l}^{(y)}$ [nm]	1.5250	1.4950	1.4000	1.4750	1.5020	1.8550
	$r_\mathrm{l}^{(z)}$ [nm]	0.6863	0.6150	0.6860	0.6800	0.8000	0.6840
	σ_l [-]	0.05	0.05	0.05	0.05	0.05	0.05
	χ_l [-]	0.6	0.6	0.6	0.6	0.6	0.6
	w_l [-]	-0.25	-0.25	-0.25	-0.25	-0.25	-0.25
	$k_\mathrm{l,l}$ [kJ/mol]	25	25	25	25	25	25
	$k_\mathrm{l,u}$ [kJ/mol]	25	25	25	25	25	25
	$s_\mathrm{l,l}$ [-]	0.02	0.02	0.02	0.02	0.02	0.02
	$s_\mathrm{l,u}$ [-]	1.05	1.05	1.05	1.05	1.05	1.05
$s_{\mathrm{s,AcO^-}}$	$r_\mathrm{s}^{(x)}$ [nm]	1.4571	1.4576	1.4559	1.6577	1.4583	1.3449
	$r_\mathrm{s}^{(y)}$ [nm]	1.5908	1.5911	1.3103	1.5981	1.5916	1.7992
	$r_\mathrm{s}^{(z)}$ [nm]	0.7442	0.6794	0.7496	0.7484	0.8639	0.7476
	σ_s [-]	0.16	0.16	0.16	0.16	0.16	0.16
	χ_s [-]	0.3	0.3	0.3	0.3	0.3	0.3
	χ_s [-]	3	3	3	3	3	3
	w_s [-]	0.5	0.5	0.5	0.5	0.5	0.5
	$k_\mathrm{s,l}$ [kJ/mol]	25	25	25	25	25	25
	$k_\mathrm{s,u}$ [kJ/mol]	25	25	25	25	25	25
	$s_\mathrm{s,l}$ [-]	0.02	0.02	0.02	0.02	0.02	0.02
	$s_\mathrm{s,u}$ [-]	2.08	2.08	2.08	2.08	2.08	2.08
$s_{\mathrm{l,AcO^-}}$	$r_\mathrm{l}^{(x)}$ [nm]	1.3780	1.3800	1.3770	1.7337	1.3770	1.4240
	$r_\mathrm{l}^{(y)}$ [nm]	1.6380	1.6450	1.2650	1.6467	1.6420	1.7410
	$r_\mathrm{l}^{(z)}$ [nm]	0.6838	0.6100	0.6850	0.6800	0.7970	0.6800
	σ_l [-]	0.10	0.10	0.10	0.10	0.10	0.10
	χ_l [-]	0.5	0.5	0.5	0.5	0.5	0.5
	w_l [-]	-1	-1	-1	-1	-1	-1
	$s_\mathrm{l,l}$ [-]	0.02	0.02	0.02	0.02	0.02	0.02
	$s_\mathrm{l,u}$ [-]	1.05	1.05	1.05	1.05	1.05	1.05

Table S16: Well-tempered Metadynamics parameter values used for the Na^+ and AcO^- growth and dissolution simulations.

	Na^+	AcO^-
W [kJ/mol]	0.2	0.2
σ_W [-]	0.06	0.06
γ [-]	8	10
τ [ps]	1	1
Δs_b [-]	0.02	0.02

NaOAc

$$s_{\mathrm{c,atom}} = \sum_i \left(1 - \frac{1}{1+\exp(-\sigma_\mathrm{c}(|\mathbf{r}_{\mathrm{c},i} - \bar{\mathbf{r}}_\mathrm{c}| - d_\mathrm{c}))}\right), \tag{S17}$$

with σ_c defining the width and d_c the position of the switching function. Vector $\mathbf{r}_{\mathrm{c},i}$ is the atom position of the i-th ion and $\bar{\mathbf{r}}_\mathrm{c}$ is the atom's position in the crystalline lattice at the kink site.

Since Na^+ is spherical, we need one switching function to define its crystallinity, i.e. CV $s_{\mathrm{c,Na+}}$. For AcO^- it is necessary to use two switching functions to account for the ion's orientation as well. For this purpose we take AcO^-'s atom C1 for crystallinity CV $s_{\mathrm{c1,AcO-}}$ and the center of mass of AcO^-'s oxygen atoms O1 and O2 for crystallinity CV $s_{\mathrm{c1,AcO-}}$.

$\bar{\mathbf{r}}_\mathrm{c}$ are easily extracted from unbiased simulations where the kink site is grown. d_c and σ_c can be interpreted as the position and width of the region of transition, in which the ion transforms from fully dissolved to crystalline. We need to define at which distance from the kink site the ion is considered dissolved and where the ion is considered crystalline. In between lies the region where the ion is in neither state but in the region of transition.

We check the distance from the kink site where the ion is fully solvated and assign values of the crystallinity CV switching functions as zero (i.e. where the ions are fully solvated). We assign CV values of one to the positions, where the ion is fully crystalline in the same way as in our previous work[27] (we also include the amplitude of the lattice vibrations to the region, where the ion is crystalline). The values between zero and one are considered to belong to values of the transition region.

All crystallinity CVs parameter values used for the reweighting process (discussed in Section S5) are shown in Table S17.

Table S17: Values of the crystallinity CVs used in the reweighting.

		pure MeOH	MeOH-PrOH			MeOH-MeCN	
		100%	80-20%	60-40%	40-60%	75-25%	50-50%
$s_{\mathrm{c,Na^+}}$	$r_{\mathrm{c}}^{(x)}$ [nm]	1.4584	1.4576	1.4567	1.6569	1.4587	1.3433
	$r_{\mathrm{c}}^{(x)}$ [nm]	1.3558	1.3572	1.5447	1.3601	1.3575	2.0351
	$r_{\mathrm{c}}^{(x)}$ [nm]	0.7506	0.6860	0.7562	0.7514	0.8713	0.7506
	σ_{c} [-]	65	65	65	65	65	65
	d_{c} [nm]	0.15	0.15	0.15	0.15	0.15	0.15
$s_{\mathrm{c1,AcO^-}}$	$r_{\mathrm{c1}}^{(x)}$ [nm]	1.4277	1.4269	1.4260	1.6877	1.4280	1.3741
	$r_{\mathrm{c1}}^{(y)}$ [nm]	1.8113	1.8127	1.0892	1.8156	1.8130	1.5796
	$r_{\mathrm{c1}}^{(z)}$ [nm]	0.7789	0.7143	0.7845	0.7797	0.8996	0.7789
	σ_{c1} [-]	80	80	80	80	80	80
	d_{c1} [nm]	0.16	0.16	0.16	0.16	0.16	0.16
$s_{\mathrm{c2,AcO^-}}$	$r_{\mathrm{c2}}^{(x)}$ [nm]	1.4084	1.4076	1.4067	1.7069	1.4087	1.3933
	$r_{\mathrm{c2}}^{(y)}$ [nm]	1.6738	1.6752	1.2267	1.6781	1.6755	1.7171
	$r_{\mathrm{c2}}^{(z)}$ [nm]	0.7506	0.6860	0.7562	0.7514	0.8713	0.7506
	σ_{c2} [-]	65	65	65	65	65	65
	d_{c2} [nm]	0.15	0.15	0.15	0.15	0.15	0.15

S5 Energy differences and WTMetaD convergence performance

For any enhanced sampling simulation, an estimate of the FES convergence performance is of key interest. Here we shall discuss the Na^+ and AcO^- growth and dissolution simulations at kink sites, which were biased with WTMetaD, for the representative case of pure MeOH solutions.

For good WTMetaD sampling, the biased CV should transition between the different states without getting stuck or needing longer and longer periods between transitioning, which otherwise would indicate a hysteresis. Figures S10a and S10b show typical simulation runs for Na^+ and AcO^- respectively at a solute mole fraction of $\chi = 0.0253$. Within 2 μs, the system transitions many times between grown and dissolved Na^+, and the same can be observed for AcO^-. No hysteresis was seen in any of the reported simulations.

Frequent transitioning between states is necessary but not sufficient for good convergence performance. The energy difference, ΔF, between crystalline and dissolved states needs to converge over time and not fluctuate with an amplitude above the energy value required to resolve the energetic differences. In this case it is necessary to have an accuracy of ΔF in dependence of the solute mole fraction χ at a level that enables us to distinguish the solubilities for the different solvent/antisolvent mixtures.

To obtain ΔF, the FES in dependence of the kink site crystallinity needs to be computed. This is done by reweighting[29] the biased simulations with the crystallinity CVs, which are discussed in Section S4.4. The FES in dependence of Na^+ crystallinity, $s_{\mathrm{c,Na+}}$, for a solute mole fraction of $\chi = 0.0253$ and simulation time $t = 2$ μs is presented in Figure S11a. As for all other biased simulations in the presented work, the first 300 ns of simulation were not used for the reweighting, since the WTMetaD bias potential changes significantly in this first time interval of the simulation. From the FES, the energy difference between crystallized and dissolved Na^+ can be obtained, $\Delta F_{\mathrm{Na+}} = F_{\mathrm{B}} - F_{\mathrm{A}}$. The time evolution of $\Delta F_{\mathrm{Na+}}$ is presented in Figure S11b for all reported Na^+ simulations in pure MeOH, run at the specified solute mole fractions. A reasonable convergence is attained around a simulation time of 1.2 μs.

Figure S11c shows the FES in dependence of the AcO^- crystallinity CVs, $s_{\mathrm{c1,AcO-}}$ and $s_{\mathrm{c2,AcO-}}$. Again, the energy difference between crystalline and dissolved AcO^- can be computed from the respective energy minima, i.e. $\Delta F_{\mathrm{AcO-}} = F_{\mathrm{C}} - F_{\mathrm{B}}$. The time evolution of $\Delta F_{\mathrm{AcO-}}$ for the specified solute mole fractions is shown in Figure S11. Again, reasonable convergence can be reached after simulation times of 1.2 μs.

As discussed in the main text, the energy difference for the dimeric unit can be obtained from summing the ΔF_{ion} of each simulation run pair of Na^+ and AcO^-, which was simulated at the same solute mole fraction, $\Delta F = \Delta F_{\mathrm{Na+}} + \Delta F_{\mathrm{AcO-}}$. The solubility can be identified at $\Delta F = 0$.

To average out energy difference fluctuations over time, the ΔF_{ion} reported in the main text and in Table S18 are the averaged values of ΔF_{ion} over the last 400 μs of simulation.

From the discussions above and results presented in the main text, we can conclude that the simulation setup has a convergence performance, that allows a reliable computation the solubilities of NaOAc in the reported solvent/antisolvent mixtures.

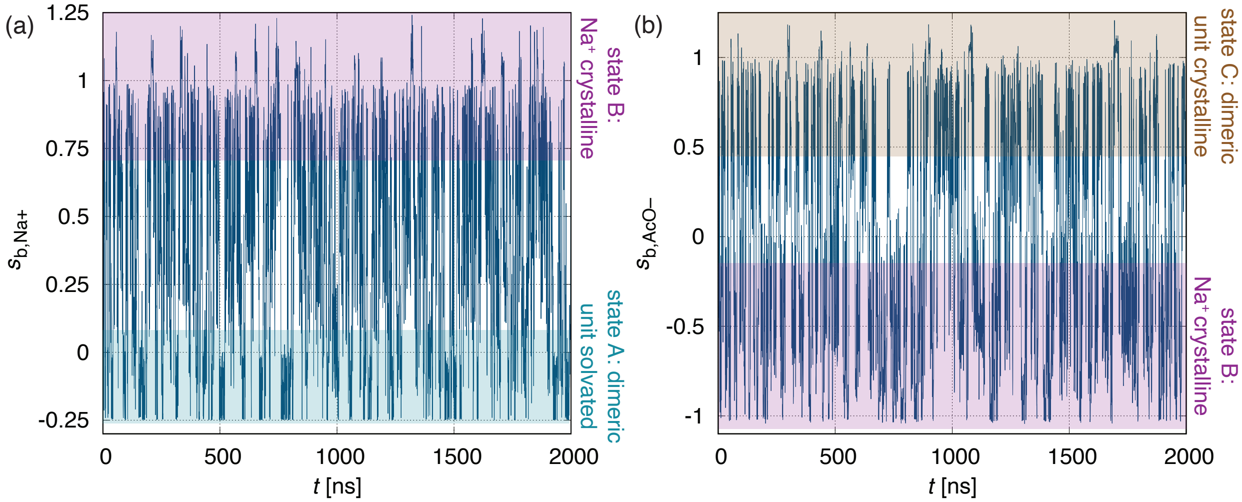

Figure S10: Time trajectories of the biased CVs for each ion in pure MeOH solution for a mole fraction of $\chi = 0.0253$. a) Biased CV of Na$^+$, $s_{\text{b,Na+}}$, vs. time; state A, where the biased dimeric unit is completely solvated, is shaded in blue and the state B, where Na$^+$ is crystalline in the dimeric unit, is shaded in purple. b) Biased CV of AcO$^-$, $s_{\text{b,AcO}-}$, vs. time; state B is again colored in purple and state C, where the biased dimeric unit is crystalline, is colored in brown.

S6 Simulation results

The numeric values of the results shown in the results section of the main text are listed in Table S18. Several simulations were repeated to test the reproducibility of the method. The averages of the ΔF_{ion} values obtained from the repetitions were used for the linear regression.

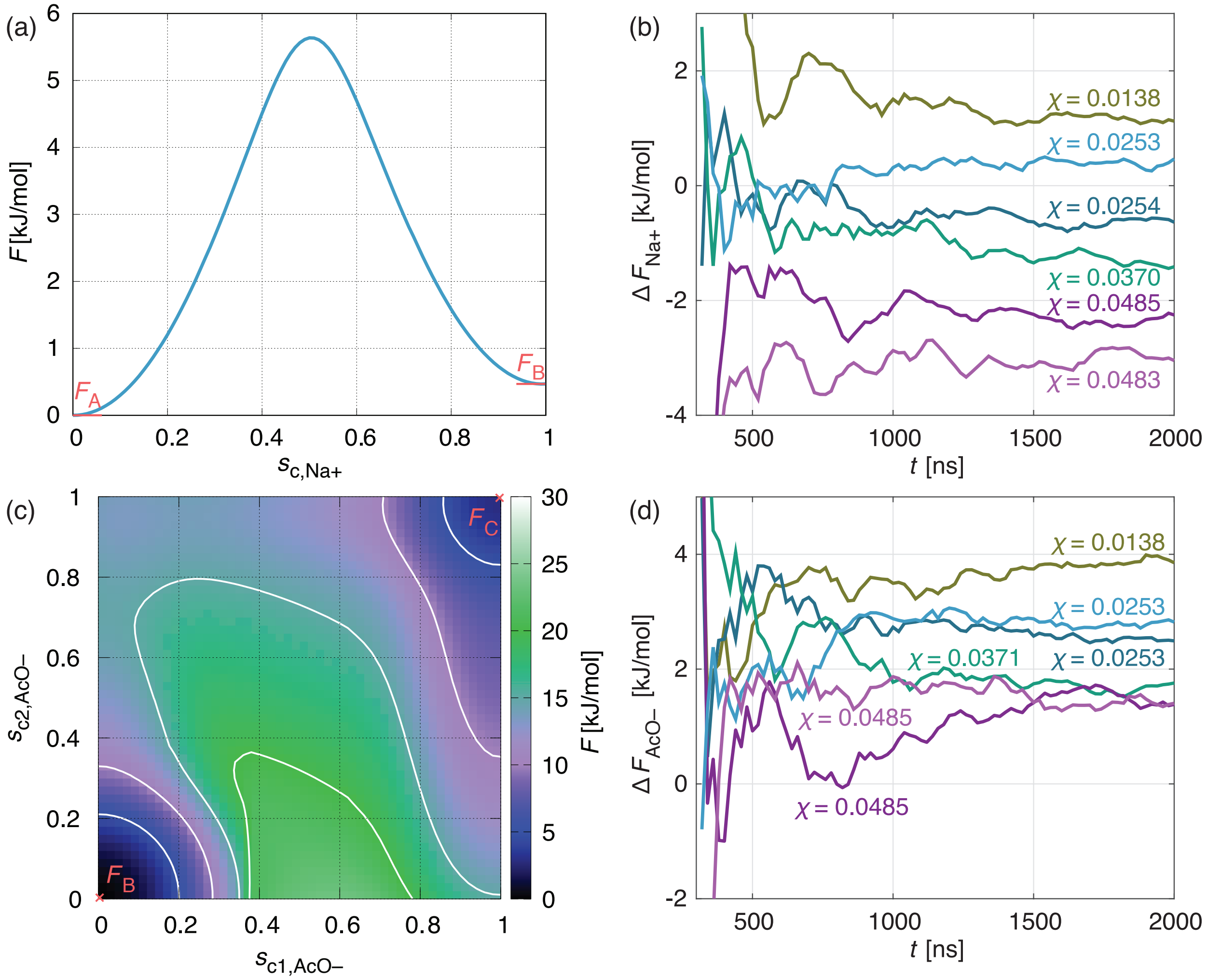

Figure S11: a) FES, F, in dependence of the crystallinity CV, $s_{\mathrm{c,Na+}}$, obtained from the Na$^+$ growth and dissolution sampling in pure MeOH solution at a solute mole fraction of $\chi = 0.0253$. The difference between the energy values of the crystalline and dissolved kink site states, F_{B} and F_{A}, yields $\Delta F_{\mathrm{Na+}}$. b) Time evolution of $\Delta F_{\mathrm{Na+}}$ for all six reported pure MeOH solution simulation runs performed at the specified solute mole fractions. c) F in dependence of the crystallinity CVs, $s_{\mathrm{c1,AcO-}}$ and $s_{\mathrm{c2,AcO-}}$, obtained from the AcO$^-$ growth and dissolution sampling in pure MeOH solution at a solute mole fraction of $\chi = 0.0253$. The difference between the energy minima F_{C} and F_{B} gives $\Delta F_{\mathrm{AcO-}}$. d) Time evolution of $\Delta F_{\mathrm{AcO-}}$ for all six reported pure MeOH solution simulations run at the specified solute mole fractions.

Table S18: Values of mole fractions and energy differences for all performed biased kink growth and dissolution simulations.

solution composition	run N°	$\chi_{\mathrm{Na+}}$ [-]	$\Delta F_{\mathrm{Na+}}$ [kJ/mol]	$\chi_{\mathrm{AcO-}}$ [-]	$\Delta F_{\mathrm{AcO-}}$ [kJ/mol]	χ [-]	ΔF [kJ/mol]
100% MeOH	1	0.0138	1.1790	0.0138	3.8549	0.0138	5.0338
	2	0.0254	-0.6460	0.0252	2.5242	0.0253	1.8782
	3	0.0253	0.3859	0.0253	2.7714	0.0253	3.1573
	4	0.0370	-1.2890	0.0372	2.3237	0.0371	0.3769
	5	0.0485	-2.3799	0.0485	1.5283	0.0485	-0.8516
	6	0.0483	-2.9770	0.0486	1.3946	0.0485	-1.5824
80-20% MeOH-PrOH	1	0.0177	0.8136	0.0175	2.8134	0.0176	3.6270
	2	0.0174	-0.0464	0.0176	3.9107	0.0175	3.8643
	3	0.0245	-0.6552	0.0245	1.9105	0.0245	1.2553
	4	0.0311	-0.1496	0.0311	1.5104	0.0311	1.3607
	5	0.0311	-1.3669	0.0315	1.4911	0.0313	0.1242
	6	0.0377	-1.4520	0.0375	-0.1456	0.0376	-1.5976
	7	0.0374	-1.9872	0.0374	0.8069	0.0374	-1.1803
60-40% MeOH-PrOH	1	0.0112	1.9627	0.0112	1.0170	0.0112	2.9797
	2	0.0117	3.3412	0.0114	0.5339	0.0116	3.8751
	3	0.0191	1.2931	0.0191	0.2854	0.0191	1.5785
	4	0.0192	0.4735	0.0192	1.0516	0.0192	1.5251
	5	0.0272	-0.3380	0.0264	-0.0116	0.0268	-0.3496
	6	0.0344	-2.6537	0.0346	-0.3976	0.0345	-3.0513
	7	0.0340	-2.7858	0.0337	-0.1634	0.0339	-2.9492
40-60% MeOH-PrOH	1	0.0065	3.9123	0.0063	0.9312	0.0064	4.8435
	2	0.0105	3.1088	0.0105	-0.3701	0.0105	2.7387
	3	0.0141	2.1516	0.0145	-0.9524	0.0143	1.1992
	4	0.0140	1.9123	0.0146	-0.6265	0.0143	1.2858
	5	0.0182	1.6744	0.0182	-2.1048	0.0182	-0.4304
	6	0.0183	1.2967	0.0183	-0.5738	0.0183	0.7229
	7	0.0215	0.2832	0.0218	-2.1561	0.0217	-1.8730
75-25% MeOH-MeCN	1	0.0092	2.0924	0.0092	3.6488	0.0092	5.7412
	2	0.0158	0.8838	0.0158	2.8862	0.0158	3.7700
	3	0.0227	-1.2024	0.0230	2.3339	0.0229	1.1314
	4	0.0299	-1.6967	0.0299	1.2920	0.0299	-0.4047
	5	0.0299	-1.6568	0.0299	2.0634	0.0299	0.4066
	6	0.0365	-2.5240	0.0365	1.0251	0.0365	-1.4989
	7	0.0365	-3.4607	0.0365	0.6874	0.0365	-2.7733
50-50% MeOH-MeCN	1	0.0022	2.9730	0.0022	2.1770	0.0022	5.1500
	2	0.0051	1.9677	0.0051	1.0203	0.0051	2.9880
	3	0.0051	2.3857	0.0051	1.6836	0.0051	4.0693
	4	0.0081	0.9459	0.0081	0.8041	0.0081	1.7500
	5	0.0110	0.2668	0.0110	0.2713	0.0110	0.5381
	6	0.0137	0.5627	0.0135	-1.1132	0.0136	-0.5505

S7 Solubility dependency on sodium acetate force fields scaling factor

As already mentioned in Section S1.2, the solubility is highly sensitive to the melting point of the crystalline compound, which is both true for real crystal systems as well as simulations. Consequently, starting off with a force field, whose melting point considerably deviates from experiments, will lead to significant deviations between simulated and experimental solubility. We have run simulations with the NaOAc force fields[4] using a scaling factor of $q = 0.840$ and compared it to the runs of $q = 0.807$. The resulting ΔF and linear interpolation are presented in Figure S12, which we have obtained from biased simulations in pure MeOH solution. Figure S12a shows the simulation results for $q = 0.840$ and Figure S12b shows the results for $q = 0.807$.

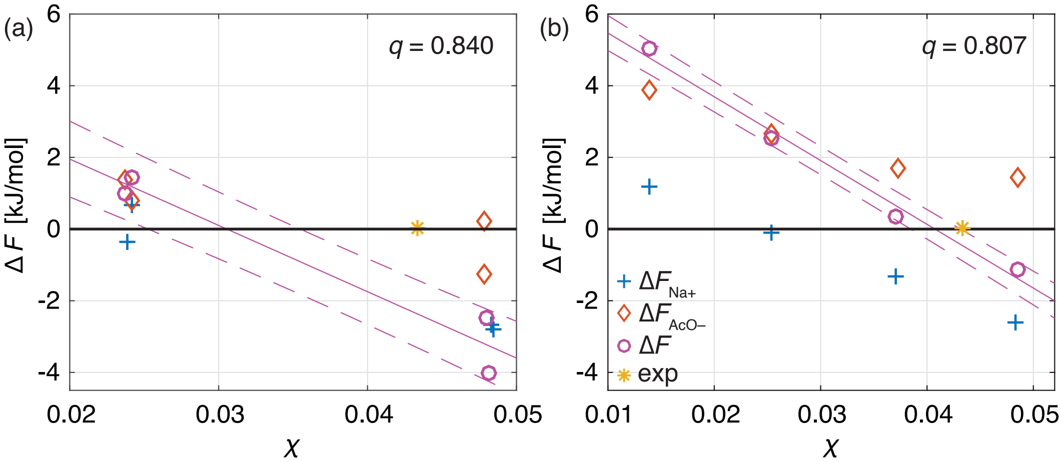

Figure S12: Sampled energy differences in dependence of solute mole fraction χ for simulations using NaOAc force fields with different charge scaling factors: a) $q = 0.840$, and b) $q = 0.807$ (Figure 3a from main text). Energy differences are shown for Na^+, $\Delta F_{\mathrm{Na+}}$ (blue crosses), AcO^-, $F_{\mathrm{AcO-}}$ (orange diamonds), and their sums, $\Delta F = \Delta F_{\mathrm{Na+}} + \Delta F_{\mathrm{AcO-}}$ (purple circles). Linear fits of the ΔF data points are shown as solid lines and the lower and upper bounds of the standard deviations are shown as dashed lines. The yellow asterisks correspond to the experimental solubility of NaOAc in pure MeOH solution.

Predicted solubilities were obtained from linear interpolation of the energy differences of the dimeric unit, ΔF, in dependence of solute mole fraction, χ, in the same fashion as in the main text. Following values were obtained for the two different NaOAc force field systems:

- ◇ $\chi^{*}_{\text{sim}}(q = 0.840) = 0.031 \pm 0.005$,
- ◇ $\chi^{*}_{\text{sim}}(q = 0.807) = 0.0407 \pm 0.0024$ (presented in main text).

Compared to the experimental solubility, $\chi^{*}_{\text{exp}} = 0.0440$, $\chi^{*}_{\text{sim}}(q = 0.840)$ has a considerable error of -30%; while $\chi^{*}_{\text{sim}}(q = 0.807)$ has an error of -7.5%, which is within the order of the simulation setup's standard deviation. While $q = 0.807$ reproduces well the experimental melting point of NaOAc, $T^{\text{exp}}_{\text{m}} = 597$ K, $q = 0.840$ leads to a melting point of $T^{\text{sim}}_{\text{m}} = 640$ K, which is around 40 K above $T^{\text{exp}}_{\text{m}}$ (i.e. 7 % relative error). A small change in the columbic interaction parameters (i.e. small relative deviation in melting temperature) leads to a large change in solubility. This comparison of results for different charge scaling factors clearly shows how important the correct melting temperature of force fields is for solubility predictions with MD simulations.

References

(1) Wang, J.; Wolf, R. M.; Caldwell, J. W.; Kollman, P. A.; Case, D. A. Development and testing of a general amber force field. *J. Comput. Chem.* **2004**, *25*, 1157–1174.

(2) Wang, J.; Wang, W.; Kollman, P. A.; Case, D. A. Automatic atom type and bond type perception in molecular mechanical calculations. *J. Mol. Graph. Model.* **2006**, *25*, 247–260.

(3) van der Spoel, D.; van Maaren, P. J.; Caleman, C. GROMACS molecule & liquid database. *Bioinformatics* **2012**, *28*, 752–753.

(4) Kashefolgheta, S.; Vila Verde, A. Developing force fields when experimental data is sparse: AMBER/GAFF-compatible parameters for inorganic and alkyl oxoanions. *Phys. Chem. Chem. Phys.* **2017**, *19*, 20593–20607.

(5) Frisch, M. J. et al. Gaussian 09, Revision B.01. 2009.

(6) Bayly, C. I.; Cieplak, P.; Cornell, W.; Kollman, P. A. A well-behaved electrostatic potential based method using charge restraints for deriving atomic charges: the RESP model. *J. Phys. Chem.* **1993**, *97*, 10269–10280.

(7) Sousa da Silva, A. W.; Vranken, W. F. ACPYPE - AnteChamber PYthon Parser interfacE. *BMC Res. Notes* **2012**, *5*.

(8) Mikhail, S. Z.; Kimel, W. R. Densities and Viscosities of 1-Propanol-Water Mixtures. *J. Chem. Eng. Data* **1963**, *8*, 323–328.

(9) Parrinello, M.; Rahman, A. Polymorphic transitions in single crystals: A new molecular dynamics method. *J. Appl. Phys.* **1981**, *52*, 7182–7190.

(10) Bussi, G.; Zykova-Timan, T.; Parrinello, M. Isothermal-isobaric molecular dynamics using stochastic velocity rescaling. *J. Chem. Phys.* **2009**, *130*, 074101.

(11) Jorgensen, W. L.; Chandrasekhar, J.; Madura, J. D.; Impey, R. W.; Klein, M. L. Comparison of simple potential functions for simulating liquid water. *J. Chem. Phys.* **1983**, *79*, 926–935.

(12) Joung, I. S.; Cheatham, T. E. Molecular Dynamics Simulations of the Dynamic and Energetic Properties of Alkali and Halide Ions Using Water-Model-Specific Ion Parameters. *J. Phys. Chem. B* **2009**, *113*, 13279–13290.

(13) Lide, D. R. *CRC Handbook of Chemistry and Physics. 73rd ed.*; CRC Press Inc.: Boca Raton, FL, 1992-1993; pp 4–96.

(14) Leontyev, I. V.; Stuchebrukhov, A. A. Electronic Continuum Model for Molecular Dynamics Simulations of Biological Molecules. *J. Chem. Theory Comput.* **2010**, *6*, 1498–1508.

(15) Doherty, B.; Zhong, X.; Gathiaka, S.; Li, B.; Acevedo, O. Revisiting OPLS Force Field Parameters for Ionic Liquid Simulations. *J. Chem. Theory Comput.* **2017**, *13*, 6131–6145.

(16) Morris, J. R.; Wang, C. Z.; Ho, K. M.; Chan, C. T. Melting line of aluminum from simulations of coexisting phases. *Phys. Rev. B* **1994**, *49*, 3109–3115.

(17) Hsu, L.; Nordman, C. E. Structures of two forms of sodium acetate. *Acta Cryst. C* **1983**, *39*, 690–694.

(18) Abraham, M. J.; Murtola, T.; Schulz, R.; Pall, S.; Smith, J. C.; Hess, B.; Lindahl, E. GROMACS: High performance molecular simulations through multi-level parallelism from laptops to supercomputers. *SoftwareX* **2015**, *1–2*, 19–25.

(19) Ewald, P. P. Die Berechnung optischer und elektrostatischer Gitterpotentiale. *Ann. Phys.* **1921**, *369*, 253–287.

(20) Darden, T.; York, D.; Pedersen, L. Particle mesh Ewald: An N log(N) method for Ewald sums in large systems. *J. Chem. Phys.* **1993**, *98*, 10089–10092.

(21) Hess, B. P-LINCS: A Parallel Linear Constraint Solver for Molecular Simulation. *J. Chem. Theory Comput.* **2008**, *4*, 116–122.

(22) Hess, B.; Kutzner, C.; van der Spoel, D.; Lindahl, E. GROMACS 4: Algorithms for Highly Efficient, Load-Balanced, and Scalable Molecular Simulation. *J. Chem. Theory Comput.* **2008**, *4*, 435–447.

(23) Perego, C.; Salvalaglio, M.; Parrinello, M. Molecular dynamics simulations of solutions at constant chemical potential. *J. Chem. Phys.* **2015**, *142*, 144113.

(24) Karmakar, T.; Piaggi, P. M.; Parrinello, M. Molecular Dynamics Simulations of Crystal Nucleation from Solution at Constant Chemical Potential. *J. Chem. Theory Comput.* **2019**, *15*, 6923–6930.

(25) Bjelobrk, Z.; Mendels, D.; Karmakar, T.; Parrinello, M.; Mazzotti, M. Solubility Prediction of Organic Molecules with Molecular Dynamics Simulations. *Cryst. Growth & Des.* **2021**, *21*, 5198–5205.

(26) Mendels, D.; Piccini, G.; Parrinello, M. Collective Variables from Local Fluctuations. *J. Phys. Chem. Lett.* **2018**, *9*, 2776–2781.

(27) Bjelobrk, Z.; Piaggi, P. M.; Weber, T.; Karmakar, T.; Mazzotti, M.; Parrinello, M. Naphthalene crystal shape prediction from molecular dynamics simulations. *CrystEngComm* **2019**, *21*, 3280–3288.

(28) Rizzi, V.; Bonati, L.; Ansari, N.; Parrinello, M. The role of water in host-guest interaction. *Nat Commun* **2021**, *12*.

(29) Tiwary, P.; Parrinello, M. A Time-Independent Free Energy Estimator for Metadynamics. *J. Phys. Chem. B* **2015**, *119*, 736–742.